Energy Nexus 5 (2022) 100031

Contents lists available at ScienceDirect

Energy Nexus

journal homepage: www.elsevier.com/locate/nexus

Thermodynamic assessment of a cogeneration system with CSP Driven-Brayton and Rankine cycles for electric power and hydrogen production in the framework of the energy and water nexus

Ehsanolah Assareh [a,*], Mohammad Assareh [b], Seyed Mojtaba Alirahmi [a], Milad Shayegh [b], Fuqiang Wang [c], Mohammadali Behrang [a], Xiaolin Wang [d]

[a] Department of Mechanical Engineering, Dezful Branch, Islamic Azad University, Dezful, Iran
[b] Mechanical Engineering Department, Jundi-Shapur University of Technology, Dezful, Iran
[c] School of New Energy, Harbin Institute of Technology at Weihai, 2, West Wenhua Road, Weihai 264209, China
[d] School of Engineering, University of Tasmania, Hobart, TAS 7001, Australia

ARTICLE INFO

Keywords:
Thermo-economic analysis
Concentrated solar power tower
Rankine cycle
Hydrogen
NSGA-II

ABSTRACT

In increasingly energy-dependent world, there is a question mark over the viability of fossil fuel resources. To tackle this issue, an integrated poly-generation system based on concentrated solar power is proposed to feed in the city grid and produce hydrogen as a clean energy carrier. Concerning the COVID-19 outbreak, all countries are in dire need of oxygen. Therefore, the produced oxygen in this system can be considered as an added value. The introduced scheme applies solar energy to supply thermal energy to a Brayton cycle. Two bottoming Rankine cycles are employed to empower a PEM electrolyzer using the residual heat from the gas turbine. The system is modelled using the Engineering Equations Solver for a comprehensive thermo-economic analysis. The exergy destruction analysis proved a significant loss of exergy by the solar field, illustrating the necessity to address this in future research. Afterwards, six design variables were selected and then optimized for the proposed system using the NSGA-II. Based on the TOPSIS approach, exergy efficiency, and capital cost rate, the objective functions were 22.2% and 272.6 $/h, respectively. Finally, a case study was performed to investigate the impact of solar irradiation and ambient temperature on system outputs.

1. Introduction

Acid rain and climate change are only a few possible repercussions of humans' overreliance on fossil fuels. Supplying around 80% of global energy demand, fossil fuels are still the number one energy source despite their environmental impact [1]. However, due to the continuous increase of both demand for energy and consciousness of fossil fuels' effects, recently, the viability of sticking to conventional fuels has been called into question [2,3]. That is why the comprehensive studies on alternative energies, including design or exergo-economic analysis of hybrid systems or the interlink between water and energy, is experiencing a booming trend [4–6]. Among various ways to exploit the renewable energy sources i.e., geothermal [7], biomass [8] and oceanic energy [9], the usage of a relatively large number of mirrors to concentrate solar energy on a central tower is a commercially available yet expensive way to enable us to feed a cycle with super-heated gas. The so-called concentrated solar power has been a topic of interest in recent academic researches, such as the work of Muhammad-Bashir et al. [10] who made a detailed comparison between a concentrated and non-concentrated PV-based system. Results reported that a concentrated PV system outperforms its counterpart by a factor between 1.5 and 3. Recent improvements on concentrated solar power (CSPs) energy systems with a special emphasis on hybridization, thermodynamic evaluation, and economic analysis were discussed by Aboelmaaref et al. [11]. Boukelia et al. [12] elaborated the main merits and demerits of using dry cooling for a CSP-based plant. The model showed almost 95% reduction in water usage by the system at the cost of a significant fall in exergetic and energetic yeild. Anvari et al. [13] assessed a system that combined biomass with CSP. The system consisted of a Brayton and Steam cycle, with a total capacity of 13.4 MW. The results signified that integrating solar power into the biomass system boosted power production by 25% and realized a 25% cut in CO_2 emission. Furthermore, the solar–biomass combined cycle was found to emit nearly 49% less CO_2 than the biomass system. According to the intermittent nature of solar power, the produced energy needs to be stored for times when it is needed. Therefore, this green energy would be converted into another green carrier, so that it can be easily transported or stored [14–16]. Ghorbani et al. [17] utilized a solar collector with Phase-Change Materials (PCMs) to supply the heat required in a thermal power station with a total capac-

* Corresponding author.
E-mail address: assareh@iaud.ac.ir (E. Assareh).

https://doi.org/10.1016/j.nexus.2021.100031
Received 23 September 2021; Received in revised form 3 November 2021; Accepted 28 November 2021
Available online 5 December 2021

Nomenclature

A_{hel}	Collector area, m^2
L	Collector length, m
$\dot{Z}$	Cost rate $/h
F1	Collector efficiency factor
$\dot{E}X$	Exergy Destruction rate, kW
$\dot{Q}$	Heat rate, kW
UL	Heat loss coefficient, W/m^2-K
h_{fi}	Heat transfer coefficient inside the receiver, W/m^2-K
M	Mass, kg
$\dot{m}$	Mass flow rate, kg•s−1
$\dot{W}$	Net power output, kW
P	Pressure, kPa
RR	Recovery ratio
G_b	Solar irradiance, W/m^2
h_x	Specific enthalpy at point x, kJ/kg
S	Specific entropy, kJ/kg.K
T	Temperature, ˚C
K	Thermal conductivity, W/m•K
V	Speed (m•s−1)
W	Width, m

Subscripts and Superscript

0	Ambient condition
avg	Average
Cond	Condenser
CSPT	Concentrated solar power tower
D	Destruction
Eva	Evaporator
pp	Evaporator pinch point, ˚C
HEX	Heat exchanger
F_R	Heat removal factor
in	Inlet condition
s	Isentropic
$\tau\alpha$	Optical efficiency
ORC	Organic Rankine cycle
out	Outlet condition
Q_L	Overall collector heat loss
P	Pump
PEM	PEM electrolyzer
SRC	Steam Rankine cycle
Tot	Total
Tur	Turbine

Greek letters

ρ	Density, kg/m^3
η	Efficiency,%
γ	Intercept factor

ity of 1063 MW. PCMs stored energy to supply the system during the night or in cases that solar energy was unavailable. A substantial portion of the dissipated energy was channelled into a multi-effect desalination system to prevent energy waste in the condenser. Capitalizing on 2571 MW worth of heat dissipated from the power station, the system managed to desalinate 8321 Kg of freshwater per second. The combined system offered 28.84% as its overall efficiency for electricity and thermal efficiency proved to be 97.18%. Exergy analysis was also implemented to investigate integrated energy systems designed based on the second law of thermodynamics. An integrated system comprising of steam and gas turbines heated by CSP was scrutinized by Azturk et al. [18]. Given the character of solar energy and its absence in the nighttime, a piece of thermal storage equipment was embedded in the design. This storage was charged by up to 9 MW worth of power over 8 h. The exergy and energy performance of the system was evaluated based on several specific parametric calculations. According to performance evaluations, the gas turbine was found to generate approximately 3.87 MW of power, whereas the steam turbine produced 1.76 MW. The results showed the exergy and energy efficiency to be around 69.2 and 37.3%, respectively. The effectiveness of nexus approaches in pursuit of a greener future has encouraged researchers to investigate renewable energies in the framework of nexus approaches [19]. Mehrjerdi, for example, modeled and optimized a stand-alone water-energy supply system in the contex of water and energy nexus empowered. The proposed system was fed by solar and wind power and it was backed up with a diesel motor to achieve higher system reliabilities [20]. Hydrogen production is also investigated in the framework of water-energy nexus by Mehrjerdi [20] and Baldinelli et al. [21].

Hydrogen storage is an emerging method to deal with fluctuating nature of clean resources as hydrogen is capable of being applied in fossil fuel-based applications or as a chemical agent in industries [22]. There are various ways to produce green hydrogen, some of which need high temperatures, like coupling high-temperature hybrid systems with Cu-Cl cycle [23,24], and some others demand lower temperature to generate hydrogen-like using proton exchange membrane (PEM) electrolyzer [25]. Usage of PEM electrolyzer would allow us to use the waste heat to produce hydrogen and oxygen and improve system efficiency. By the way, relying on hydrogen not only enables us to deal with solar intermittency but also aids waste-to-energy nexus, helping in resolving grave issues like global warming [26]. Alirahmi et al. [27] proposed a novel CSP-derived hybrid system for hydrogen and electricity generation. The system was thoroughly analyzed and presented exergetic efficiency of 60.4% and cost rate of 117.5 $/GJ. In imperfect processes, the waste was high in the amount [28]. Therefore, to address this problem, the application of organic Rankine cycles (ORC) was studied because they were apt to exploit low-exergy input so they can be rated as viable options to recover waste-heat and generate power at high- and low-temperature heat sources like biogas and solar ponds. Their functionality and performance have been explored through various studies [29–31]. Moradi Nafchi et al. [32] tried the production of hydrogen by integration of a heliostat-based CSP, PEM electrolyzer, and thermal energy storage systems. They proved that the implementation of a thermal energy storage system reduced the overall energetic and exergetic efficiencies to 23.1% and 45%, respectively. Salehi et al. [33] evaluated a multi-generation power plant using biomass with a heat recovery steam generator, Stirling engine, and an ORC then performed a thermodynamic analysis. Energy, exergy, and environmental evaluations were carried out for the proposed systems. According to the results, the fuel cell and biomass contributed significantly to the destruction of exergy. It was also demonstrated that the maximum exergy efficiency was 50.18% for a 0.289 ton/MWh carbon dioxide emission.

Along with all problems caused by the recent COVID-19 pandemic, investigation of energy consumption data during the lockdown could provide us with an asset to estimate energy consumption in the future. As illustrated by Rouleau and Gosselin [34], the consumption pattern turned to be more distributed during the day rather than concentrated. This change was good for renewables, especially solar-based ones, which were more available during the day as it reduced the need for storage, making them more economically viable.

Based on the literature, while a plethora of studies have explored the thermodynamic and economic analysis of co-generations, multi-objective optimization of a system consists of 2 bottoming cycles namely a steam Rankine cycle (SRC) and an organic Rankine cycle (ORC), has not been yet fully investigated. The proposed system is comprised of a Brayton cycle, powered by CSP, and a PEM electrolyzer empowered

by an SRC and ORC. One novelty of this study lies in the application of CSP as the combustion chamber for the gas turbine. Due to the pre-mentioned expectations that the consumption pattern will change and most of the electricity need would happen to be during the daytime, the system mainly aimed to back up the grid during the daytime. The system's elements are deeply analyzed from energy, exergy, and economic (3E) points of view in the framework of the energy nexus approach. To mitigate problems regarding intermittency of solar energy, hydrogen, as the energy career, is produced through water electrolysis. Along with stabilizing the grid, hydrogen is also produced through a water electrolysis process, using waste heat energy. This hydrogen would be stored for further uses to mitigate the problems regarding intermittency of solar irradiation. Hydrogen production processes from renewables are considered globally hot topics; yet, studies on optimizing them are insufficient. Moreover, according to the huge shortage of pure oxygen for healthcare needs as a result of the COVID-19 outbreak, oxygen is also produced and stored. Following the thermo-economic analysis, the design parameters are optimized for the very first time for the presented system by applying NASGA-II. An exergy destruction analysis is also provided to pinpoint the components whose improvement needs to be prioritized. After a detailed cost analysis, a case study is performed to study the effect of ambient temperature and solar irradiation on the system performance. In short, the primary objectives and innovations of this study are:

- An innovative configuration is introduced for power and hydrogen generation, using a double-stage Rankine cycle comprising an electrolyzer and a solar energy system;
- Thermo-economic analysis of the proposed system
- Multi-objective optimization to define the optimum for objective functions;
- Exergy destruction analysis to specify the primary sources of exergy destruction
- Oxygen production to supply health care system
- A case study to assess the effect of solar irradiation and ambient temperature

2. System description

The schematic diagram of the proposed energy cogeneration system and its components are shown in Fig. 1. The system consists of several subsystems, including a CSP, a Brayton cycle, an SRC, an ORC, and a PEM electrolyzer. The goal for implementing two bottoming ORC is to maximize the use of residual heat from the gas turbine. First, ambient air is compressed (stage 1) and delivered to the CSP tower. The compressed air receives heat from heliostats that concentrate the solar radiation on the tower. The compressed high-temperature gas flows through the gas turbine in the Brayton cycle and expands to generate work. Afterwards, the gas passes through a heat exchanger (HEX) (stage 4) to heat the working fluid in a SRC for more power production. Moreover, to exploit the remaining heat, an ORC turbine is employed after the SRC. Finally, powered by turbines 2 and 3, the electrolyzer produces oxygen and hydrogen and stores them for later use. As it was stated in the literature, the power consumption tends to be more distributed during the day, and the proposed system can perform at its maximum efficiency. Therefore, the system can be used either for industries where the working hour is limited to the daytime or feeding the grid during the daytime.

3. Thermodynamic analysis

For the recommended multi-generation system, the laws of conservation of mass and energy are employed to analyze the system thermodynamically. Considering each system component as a control volume, the conservation of mass and energy are:

$$\sum \dot{m}_{in} = \sum \dot{m}_{out} \tag{1}$$

Table 1
Input parameters for system modeling [35–38].

Parameters	Value	Unit
Heliostat field;		
η_{hel}	0.71	–
A_{hel}	121	m^2
N_{hel}	320	–
DNI	850	W/m^2
A_r	60	m^2
ε	0.88	–
V	5	m/s
Brayton cycle;		
T_0	25	°C
P_0	101.3	kPa
T_3	850	°C
R_p	9.67	–
$\eta_{Gas\ Turbine}$	0.85	--
$\eta_{comprsor}$	0.85	–
Steam & organic Rankine cycles;		
P_7	3151.38	
P_9	101.88	kPa
$\eta_{Turbine2,3}$	0.85	kPa
η_{Pump}	0.8	–
Pinch Point Evaporator	5.22	–
Pinch Point Condenser	5	°C
T_{11}	86.26	°C
T_{13}	35	°C
		°C
		°C
PEM electrolysis;		
P_{o2}	101.325	kPa
P_{H2}	101.325	kPa
T_{PEM}	80	°C
$E_{act,\ a}$	76	kJ/mol
$E_{act,\ c}$	18	kJ/mol
λ_a	14	–
λ_c	10	–
D	100	Mm
J_a^{ref}	1.7×10^5	A/m^2
J_c^{ref}	4.6×10^3	A/m^2
F	96.486	C/mol

$$\dot{Q} - \dot{W} = \sum (\dot{m}h)_{out} - \sum (\dot{m}h)_{in} \tag{2}$$

The assumptions for energy analysis are as below:

- The system performs under steady-state conditions.
- Isentropic efficiencies are assumed for turbines and pumps.
- The pressure drops are negligible in pipelines and heat exchangers.
- The condenser outlet is assumed to be a saturated liquid; on the other hand, the evaporator outlet is saturated steam ($x = 1$).
- Potential and kinetic energies were ignored.

EES was used to solve all equations for the different cycle components. The initial input parameters are represented in Table 1 and are further used for optimization purposes. Note that, although the illustrated temperatures are in Celsius scale, in formulas and codes they are converted in *K*elvin scale.

3.1. Solar thermal power plant with a central receiver

Solar intensity is an important parameter to evaluate solar energy systems. This parameter is denoted by direct of normal irradiance (*DNI*) in the present study and is measured in $W \bullet m^{-2}$. The variations of this factor are sinusoidal during the day, reaching a peak during the day. Heat transfer from the heliostat to the solar collector is obtained as follows [39]:

$$\dot{Q}_h = \eta_h \times A_{hel} \times N_{hel} \times DNI \tag{3}$$

Where η_h is the solar efficiency of the heliostat, A_{hel}, N_{hel} and *DNI* are the surface area of one heliostat, the number of reflectors, and the solar

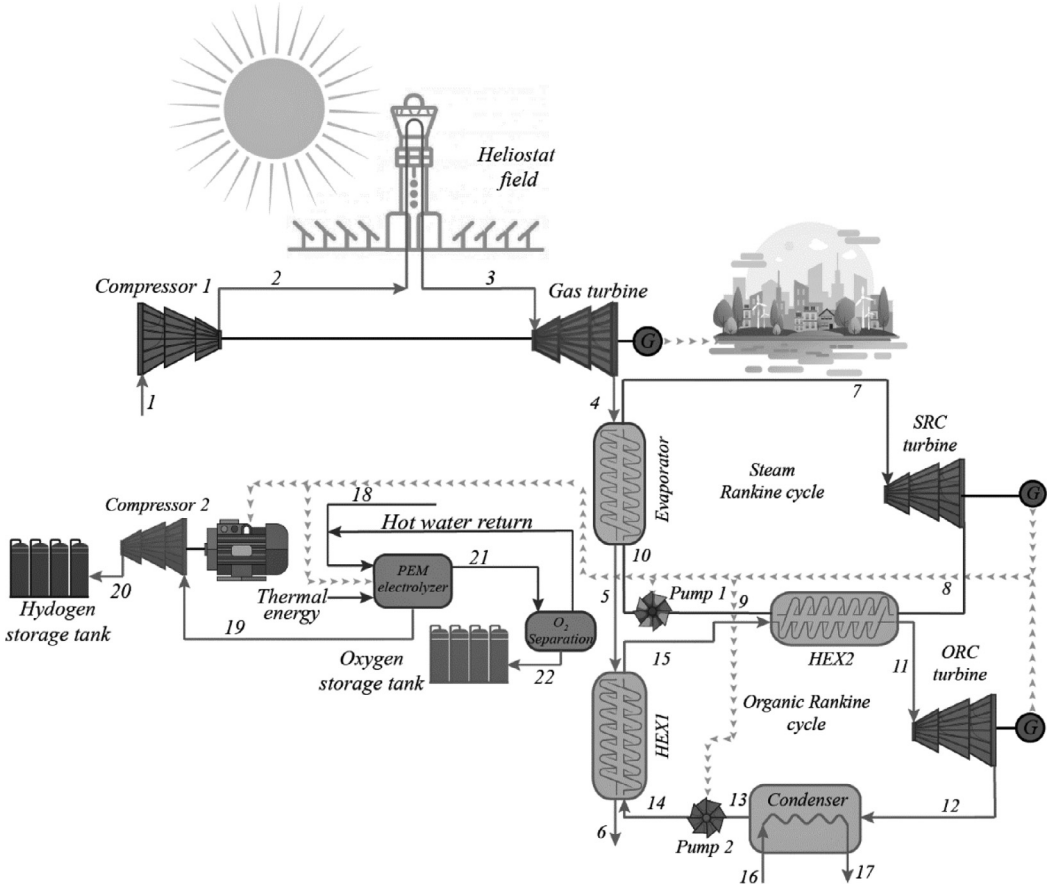

Fig. 1. Schematic of the proposed configuration system.

Table 2
Equations for energy and exergy balance for components of the suggested system [49–52].

Component	Energy balance equations	Exergy destruction rate equations
Compressor	$\dot{W}_{comp} = \dot{m}_1(h_2 - h_1)$	$\dot{E}x_{comp} = \dot{E}x_1 + \dot{w}_{comp} - \dot{E}x_2$
Gas turbine	$\dot{W}_{gas-tur} = \dot{m}_3(h_3 - h_4)$	$\dot{E}x_{gas-tur} = \dot{E}x_3 - \dot{E}x_4 - \dot{w}_{gas-tur}$
Steam turbine	$\dot{W}_{steam-tur} = \dot{m}_7(h_7 - h_8)$	$\dot{E}x_{steam-tur} = \dot{E}x_7 - \dot{E}x_8 - \dot{w}_{steam-tur}$
ORC turbine	$\dot{W}_{ORC} = \dot{m}_{11}(h_{11} - h_{12})$	$\dot{E}x_{ORC-tur} = \dot{E}x_{11} - \dot{E}x_{12} - \dot{w}_{ORC-tur}$
Pump 1	$\dot{W}_{P-1} = \dot{m}_9(h_{10} - h_9)$	$\dot{E}_{Pump-1} = \dot{E}x_9 + \dot{w}_{Pump-1} - \dot{E}x_{10}$
Pump 2	$\dot{W}_{P-2} = \dot{m}_{13}(h_{14} - h_{13})$	$\dot{E}x_{Pump-2} = \dot{E}x_{13} + \dot{w}_{Pupm-2} - \dot{E}x_{14}$
HEX 1	$\dot{Q}_{HEX-1} = \dot{m}_{10}(h_7 - h_{10})$	$\dot{E}x_{EVA-1} = \dot{E}x_4 + \dot{E}x_{10} - \dot{E}x_7 - \dot{E}x_5$
HEX 2	$\dot{Q}_{HEX-2} = \dot{m}_{15}(h_{11} - h_{15})$	$\dot{E}x_{EVA-2} = \dot{E}x_{15} + \dot{E}x_8 - \dot{E}x_9 - \dot{E}x_{11}$
HEX 3	$\dot{Q}_{HEX-1} = \dot{m}_{14}(h_{15} - h_{14})$	$\dot{E}x_{HEX} = \dot{E}x_{14} + \dot{E}x_5 - \dot{E}x_6 - \dot{E}x_{15}$
Condenser	$\dot{Q}_{cond} = \dot{m}_{12}(h_{13} - h_{12})$	$\dot{E}x_{Cond} = \dot{E}x_{12} + \dot{E}x_{16} - \dot{E}x_{13} - \dot{E}x_{17}$

Table 3
The function of cost rate components in the present research system.

Component	Purchased cost ($)
Gas-turbine	$Z_{Gas-tur} = (\frac{1536*\dot{m}_1}{0.92-\eta_{Gas-tur}}) \times \ln(\frac{P_3}{P_4}) \times (1 + \exp(0.36 \times T_3 - 54.4))$
Steam-turbine	$Z_{Steam-tur} = 4750 \times (\dot{w}_{Steam-tur})^{0.75}$
ORC-turbine	$Z_{ORC-tur} = 4750 \times (\dot{w}_{ORC-tur})^{0.75}$
HEX	$Z_{HEX} = 276 \times (A_{HEX})^{0.88}$
Pump	$Z_{Pump} = 3500 \times (\dot{w}_{Pump})^{0.41}$
Compressor	$Z_{Comp} = (\frac{(71.1 \times \dot{m}_1}{0.9-\eta_{Comp}}) \times (\frac{P_2}{P_1}) \times (\ln \frac{P_2}{P_1})$
Condenser	$Z_{Cond} = 1773 \times \dot{m}_{12}$
Heliostat	$Z_{Heliostat} = 150 \times A_{Hel} \times N_{Hel}$

Table 4
Design variables and their variations.

Upper bound	Lower bound	Parameter
15	5	$\mathbf{r_p}$
500	250	$\mathbf{N_{hel}}$
4000	1000	$\boldsymbol{p_7}$
120	80	$\boldsymbol{p_8}$
90	70	$\mathbf{T_{11}}$
10	3	$\mathbf{PP_{HEX,1}}$

intensity, respectively. Given the losses due to conduction, convection, and radiation at the collector, not all the thermal energy is transferred into the system. The heat transfer losses are calculated by [40]:

$$\dot{Q}_{loss} = h_a A_r (T_r - T_0) + \sigma \varepsilon A_r (T_r^4 - T_0^4) \quad (4)$$

h_a in this equation states the convection heat transfer coefficient of air, ε is the absorber emissivity, and σ denotes the Stefan–Boltzmann constant. h_a can be obtained from the following empirical relation [39]:

$$h_a = 10.45 - v_{wind} + 10\sqrt{v_{wind}} \quad (5)$$

Where V_{wind} denotes the wind speed in "m•s^{-1}". Finally, the heat transfer rate from the solar collector to the compressed air is [40]:

$$\dot{Q}_r = \dot{Q}_h - \dot{Q}_{loss} \quad (6)$$

$$\dot{Q}_r = \dot{m}_2 \times (h_3 - h_2) \quad (7)$$

3.1. PEM electrolyzer

Several researchers have studied and optimized various hydrogen production methods like thermochemical hydrogen production, hybrid

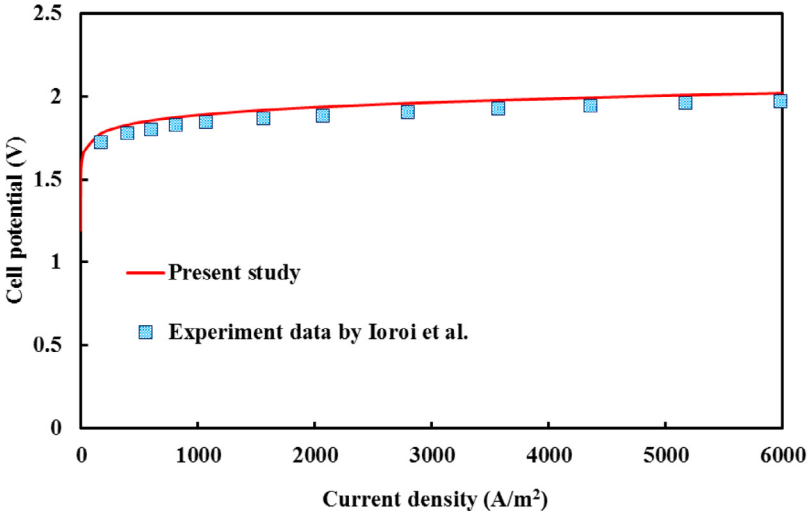

Fig. 2. Comparison of the current model of PEM electrolyzer with experimental data.

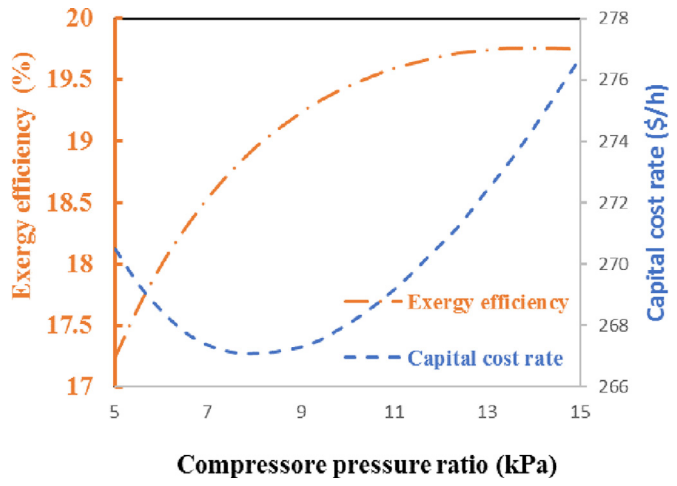

Fig. 3. Influence of compressor pressure ratio on exergy efficiency and capital cost rate.

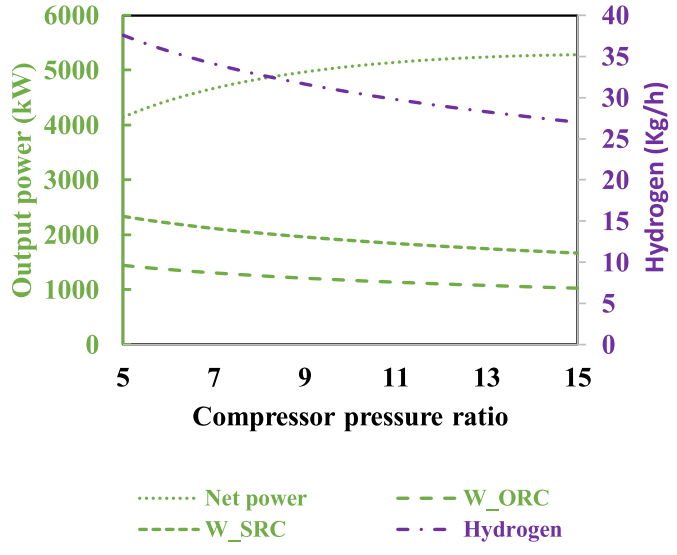

Fig. 4. Influence of compressor pressure ratio on output power, and hydrogen production.

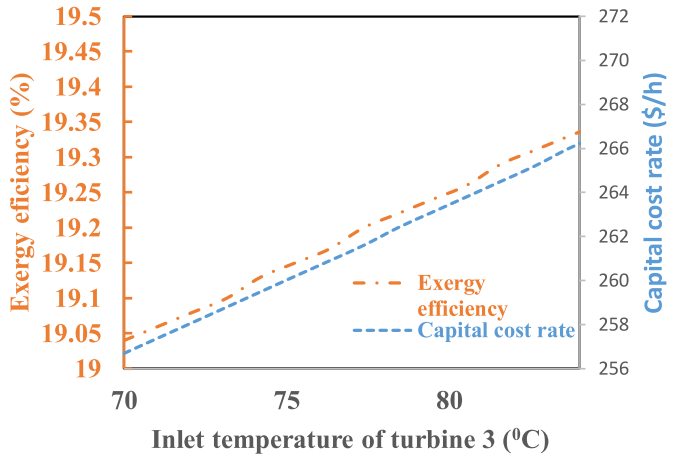

Fig. 5. Impact of ORC turbine inlet temperature on exergy efficiency and capital cost rate.

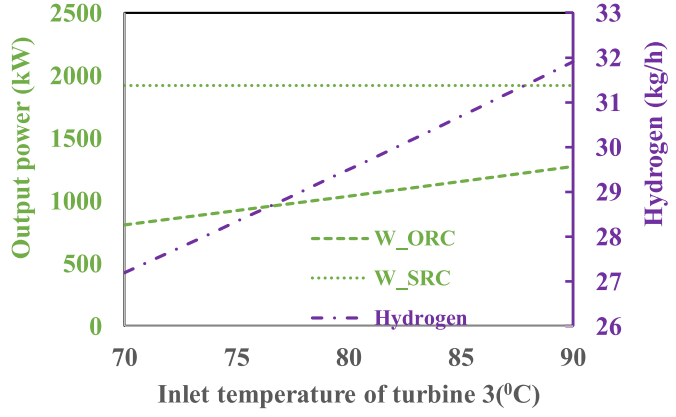

Fig. 6. Effect of ORC inlet temperature on output power, and hydrogen production rate.

cycles, and algae methods [24,41]. Hydrogen, in this study, is produced through a process called water electrolysis, which enables the system to store the energy for the time that solar energy is unavailable. This water electrolysis is polymer electrolyte membrane (PEM) electrolysis, which is the decomposition of water in a cell comprised of solid polysulfonated membranes. On the left-hand side of Fig. 1, the schematic diagram of an

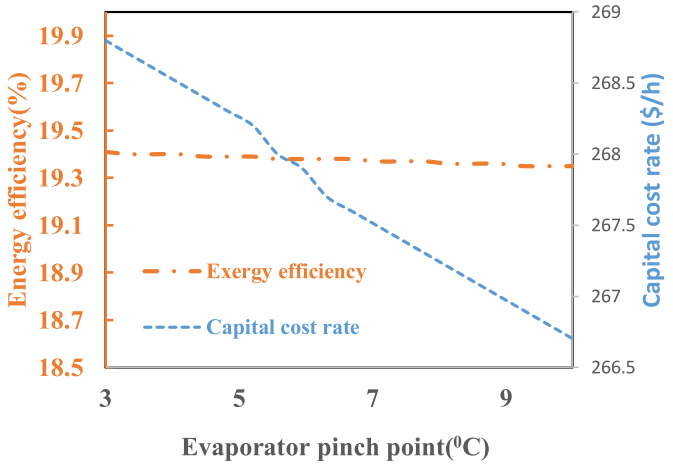

Fig. 7. Impact of the evaporator 1 pinch point on exergy efficiency and capital cost rate.

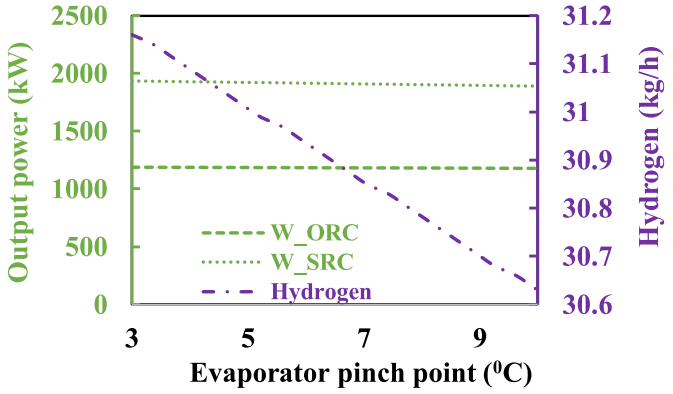

Fig. 8. Effect of the evaporator 1 pinch point on output power by SRC and ORC, and hydrogen production rate.

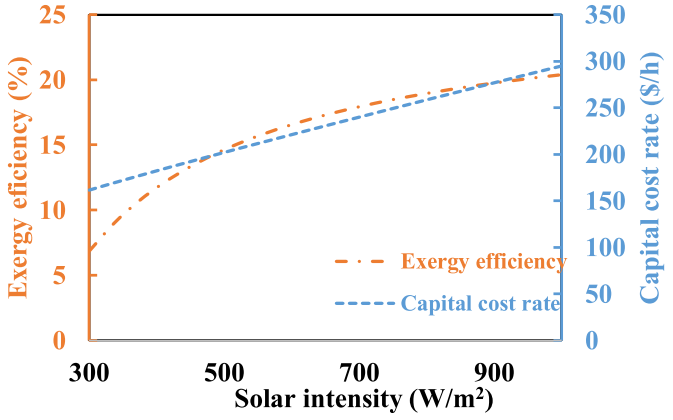

Fig. 9. Influence of solar intensity on the exergy efficiency and capital cost rate.

electrolyzer is presented. In this stage, electricity is provided to the electrolyzer to pose electrochemical reactions. Energy required to perform the electrolysis process can be obtained from:

$$\Delta H = \Delta G + T\Delta S \tag{8}$$

The values of oxygen, water, and hydrogen properties are available in thermodynamic tables [42]. The mass flow rate of output hydrogen is assessed by [43]:

$$\dot{N}_{H2:out} = \frac{J}{2F} = \dot{N}_{H2:reacted} \tag{9}$$

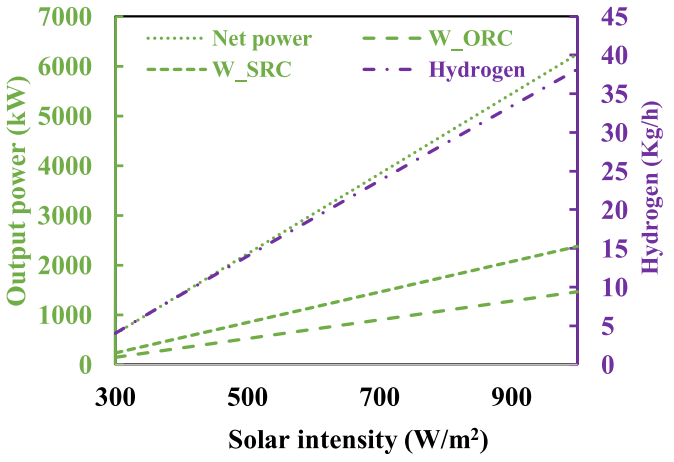

Fig. 10. Influence of solar intensity on the output power and hydrogen production rate.

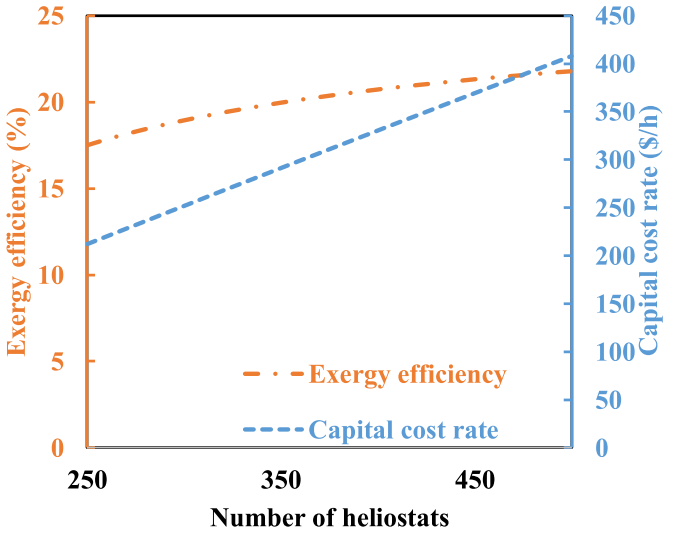

Fig. 11. Effect of the number of heliostats on the exergy efficiency and cost ratio.

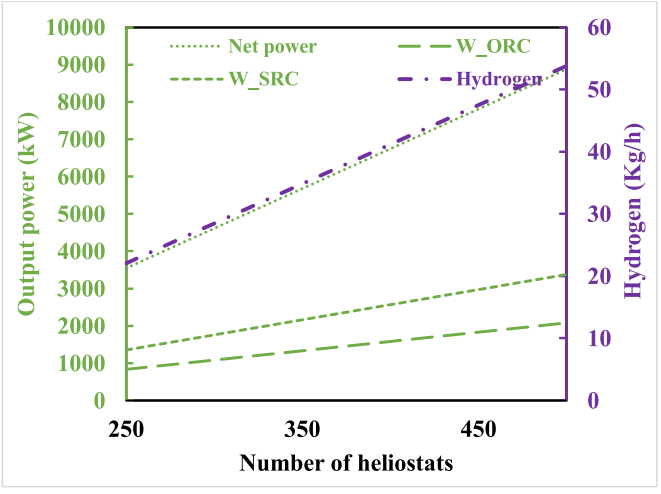

Fig. 12. Effect of the number of heliostats on the output power and PEM products.

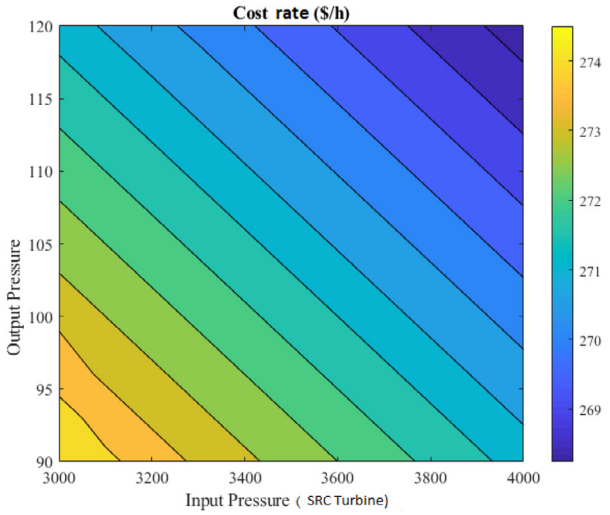

b) Effect of inlet and outlet pressure of SRC turbine on cost ratio

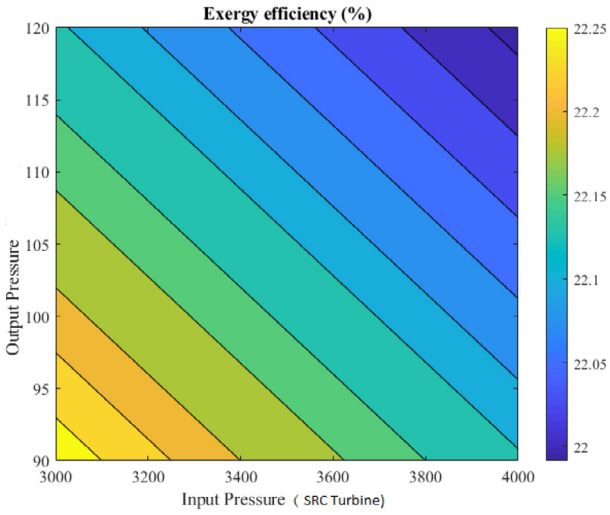

a) Effect of inlet and outlet pressure of SRC turbine on exergy efficiency

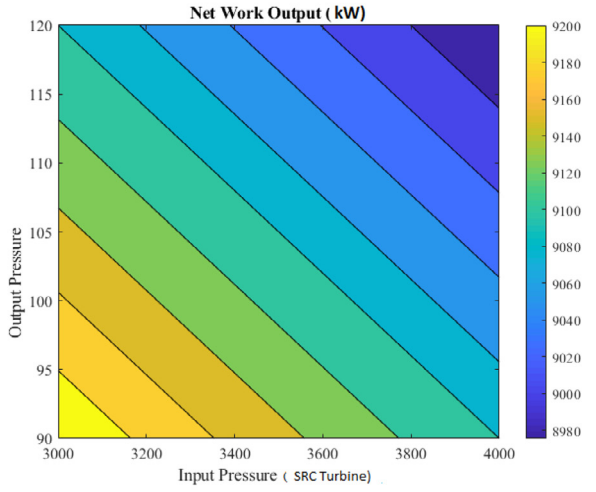

d) Effect of inlet and outlet pressure of SRC turbine on net power output

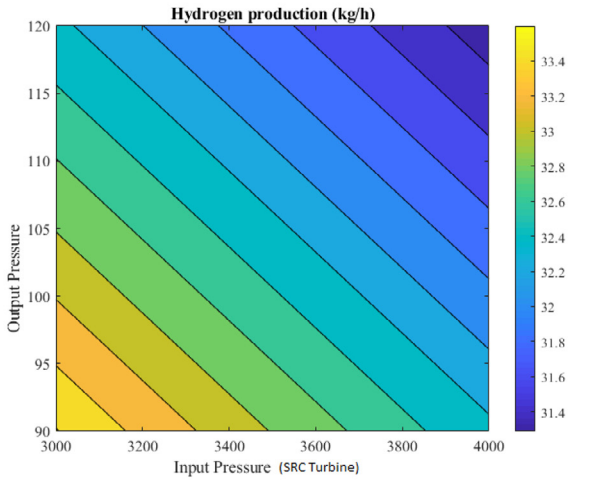

c) Effect of inlet and outlet pressure of SRC turbine on hydrogen production.

Fig. 13. Effect of SRC turbine inlet and outlet pressure on system performance.

$$\dot{N}_{O2:out} = \frac{J}{4F}$$

In the above equations, J and F denote current density and the Faraday constant, respectively. The electrical energy enters into the electrolyzer at the rate of [36]:

$$Ex_{electric} = E_{electric} = Jv \tag{10}$$

Due to Ref. [43] V is defined as:

$$V = V_0 + V_{act,a} + V_{ohm} \tag{11}$$

V_0 is obtainable using the Nernst equation [44]:

$$V_0 = 1.229 - 8.5 \times 10^{-4}\left(T_{PEM} - 298\right) \tag{12}$$

As depicted in Table. 1, the temperature for PEM is 353 °K. The upshot of transportation of hydrogen ions along the membrane is ohmic overpotential in the proton exchange membrane. Membrane temperature, thickness, and degree of humidification are determining factors of the ionic resistance of the membrane. The local ionic conductivity would be defined as bellow [43]:

$$\sigma_{PEM}[\lambda(x)] = [0.5139\lambda(x) - 0.326]\exp\left[1268\left(\frac{1}{303} - \frac{1}{T}\right)\right. \tag{13}$$

$$\lambda(x) = \frac{\lambda_a - \lambda_c}{D}x + \lambda_c \tag{14}$$

so, the ohmic resistance can be achieved by [43]:

$$R_{PEM} = \int_0^D \frac{dx}{\sigma[\lambda(x)]} \tag{15}$$

Besides, to obtain V_{ohm} use:

$$V_{ohm} = J R_{PEM} \tag{16}$$

When net current deviates from the equilibrium state, an activation overpotential appears. The equations for the electrode's activation overpotential and exchange current density are [36,43]:

$$V_{act,t} = \frac{RT}{F}\sinh^{-1}\left(\frac{J}{2J_{0,i}}\right), i = a, c \tag{17}$$

$$J_{0,i} = J_i^{ref}\exp\left(-\frac{E_{act,i}}{RT}\right),\ i = a, c \tag{18}$$

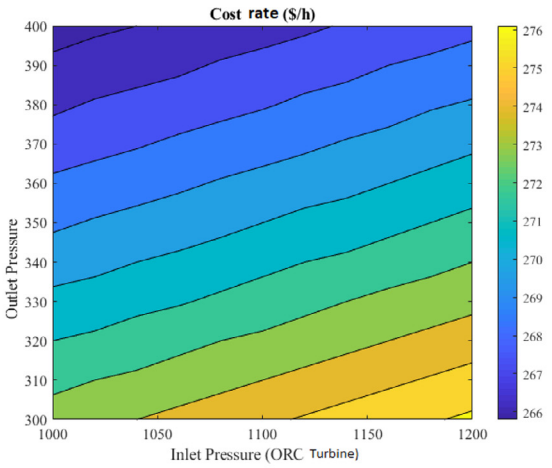

b) Effect of inlet and outlet pressure of ORC turbine on cost ratio

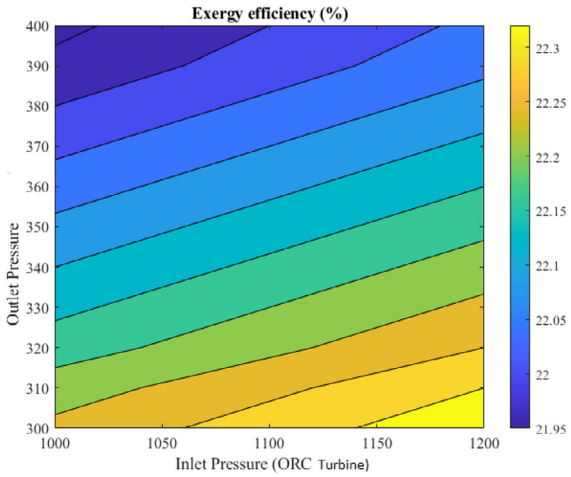

a) Effect of inlet and outlet pressure of ORC turbine on exergy efficiency

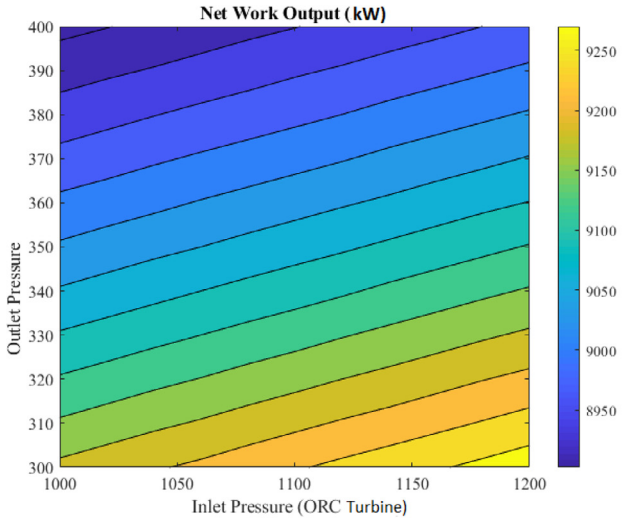

d) Effect of inlet and outlet pressure of ORC turbine on net power output

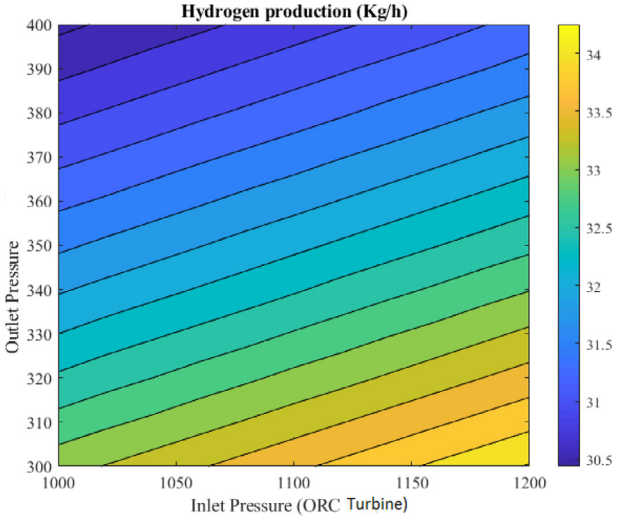

c) Effect of inlet and outlet pressure of ORC turbine on hydrogen production.

Fig. 14. Effect of ORC turbine inlet and outlet pressure on system performance.

Complementary information can be found in ref. [22,27]

3.3. Energy, exergy, and economic analysis

3.3.1. Energy analysis

The first law of thermodynamics, which only accounts for the quantity of energy, states [45]:

$$\dot{Q} - \dot{W} = \sum (\dot{m}h)_{out} - \sum (\dot{m}h)_{in} \tag{19}$$

In the above formula, $\dot{Q}$ states the heat transfer rate, the work rate, and enthalpy are represented by $\dot{W}$ and h, respectively. The first law of thermodynamics ignores variations in the potential and kinetic energy under steady-state conditions.

3.3.2. Exergy analysis

Exergy is the measure of the energy's quality and a useful asset optimizing a system. In other words, exergy refers to the maximum work that can be derived from a system. Contrary to energy, which can be neither created nor destroyed, the more entropy is produced, the more exergy would be destroyed [38]. In the thermodynamic analysis, exergy is discussed in physical, chemical, potential, and kinetic varieties. The present study considers only physical and chemical exergy. Therefore, the exergy rate balance is expressed as follows:

$$\dot{E}x = \dot{E}x_{ph} + \dot{E}x_{ch} \tag{20}$$

The physical exergy is calculated from [46]:

$$\dot{E}x_{ph} = \dot{m}\left[(h - h_0) - T_0(s - s_0)\right] \tag{21}$$

Given the chemical reaction in the electrolyzer, chemical exergy was also taken into account. Chemical exergy is expressed as follows [47].

$$\dot{E}x_{ch} = \dot{n}\left[\left(\sum_i y_i \overline{ex}_i^{ch.0} + RT_0 \sum_i y_i \ln\left(y_i\right)\right)\right] \tag{22}$$

Where $\overline{ex}_i^{ch.0}$ denotes standard chemical exergy.

Further, the exergy balance, with D representing the exergy destruction, for a single component is as follows [48]:

$$\dot{E}x_Q + \sum_{in} \dot{E}x_{in} = \dot{E}x_w + \dot{E}x_D + \sum_{out} \dot{E}x_{out} \tag{23}$$

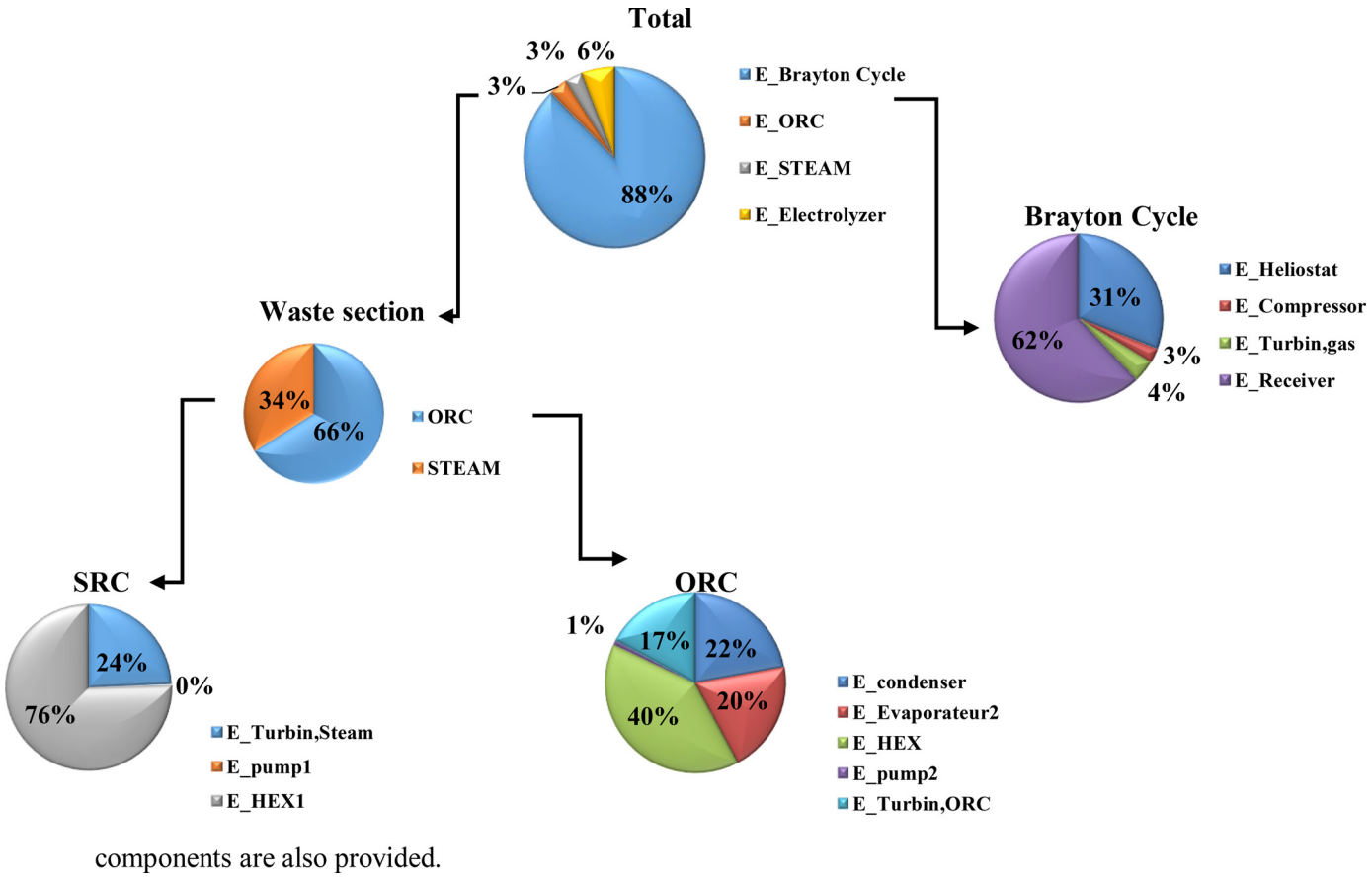

components are also provided.

Fig. 15. Rate of exergy destruction in the proposed systems' components (kW).

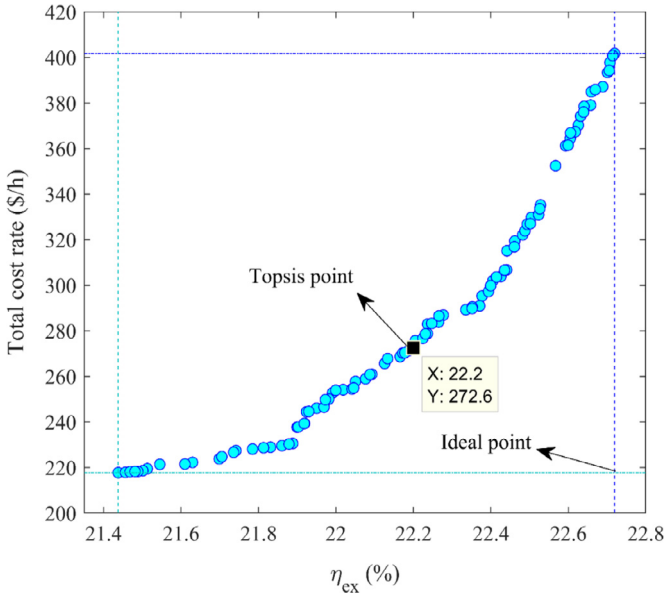

Fig. 16. Pareto frontier obtained from the optimal solutions of the proposed system.

Table 2 presents the energy and exergy balance for all pieces of equipment in the proposed system.

3.3.3. Economic analysis

The integrated system introduced here consists of several subsystems; the cost function of each is presented in Table 3.

3.4. Validation

Considering that there is no precedent for the proposed system, its components are validated individually. For this purpose, validation is performed by comparing the fundamental components with the experimental data in the literature. For verification, the PEM electrolyzer model in this study is compared with that of Ioroi [53]. Although few deviations do exist, as illustrated in Fig. 2, the results from the present study agrees well with the experimental data. This comparison results indicate that the presented model is highly reliable.

4. Results and discussion

The following subsections elaborate on the results of modeling the presented system via EES software. The following parametric study deeply investigates the effects of various design variables on the system performance.

4.1. Effect of compressor pressure ratio

Figs. 3 and 4 show the effects of the compressor pressure ratio on the exergy efficiency, capital cost rate, power output and hydrogen generation. As shown in Fig. 3, the overall exergy efficiency holds a positive correlation with the compressor pressure ratio. Concerning the existence of the term related to the power output in the exergy efficiency equation's numerator, both exergy efficiency and the generated power of the

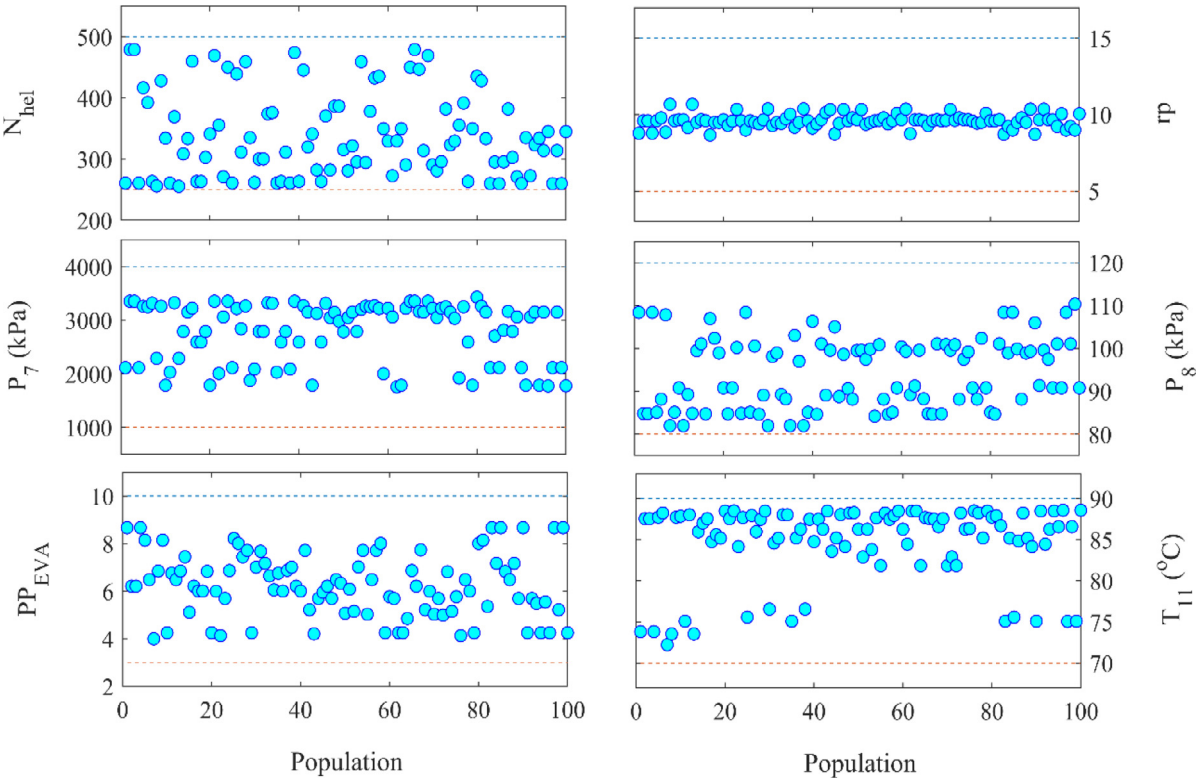

Fig. 17. Scatter distribution of decision variables.

system display similar behavior. Moreover, the capital cost of the system fluctuates along with changes in pressure ratio. For a pressure ratio of 8, the system cost reaches a minimum of 267 $/h, which goes up by elevating the pressure ratio. This parabolic behavior relates to the positive correlation between the generated power and cost ratio. In fact, by setting the inlet and outlet pressure of SRC turbine constant (our design variables), the compressor pressure ratio makes its most effective on the Brayton cycle since by increasing it, contrary to the Brayton cycle, whose mass flow rate significantly increases, little change in mass flow rate of bottoming cycles takes place. To elaborate, concerning Fig. 4, while the generated power in the ORC and SRC sees a decrease by elevating the compressor pressure ratio, the Brayton cycle generated power experiences an incremental trend. As it was mentioned earlier, at lower pressure ratios, the effect of reduction in generated power and cost ratio is dominant; yet, at greater pressure ratio values, the generated power and cost ratio are mostly under influence of the Brayton cycle due to its greater mass flow rate.

Fig. 4 also examines how the amount of produced power, hydrogen and oxygen are under the influence of the pressure ratio of the compressor, it is clear that increasing this ratio from 5 to 15 results in a reduction in PEM electrolyzer products.

4.2. Effect of the inlet temperature of orc turbine

Figs. 5 and 6 show how capital cost rate, exergy efficiency, output power, and hydrogen production are influenced by the inlet temperature of turbine 3. Based on these two figures, an increase in the input temperature of the fluid to the ORC leads to enthalpy to rise as well. Therefore, the output power of turbine 3 is enhanced from 760.6 to 1293 kW. Enthalpy in the SRC remains relatively stable in various temperatures. As a result, its power output remains unchanged. As the ORC output power increases and more power is generated, hydrogen production experiences a rise from 26.5 to 32 kg/h. The appearance of the term related to output work in the numerator of the equation for total exergy means that by increasing the inlet temperature of turbine 3, the power output and costs rise.

4.3. Effect of the evaporator 1 pinch point

Figs. 7 and 8 illustrate the influence of the pinch point of evaporator 1 on system performance. The increase in the pinch point of evaporator 1 from 3 to 10 slightly decreases its heat transfer. Reduction in heat transfer from evaporator 1 to the working fluid reduces SRC output power from 1187 to 1177 kW. Owing to the reduced heat delivered to the SRC, the ORC will also receive less amount of heat, causing a decline in its PEM products. The reduction in both generated power and PEM electrolyzer products reduces the system costs from 268 $/h to 266$/h.

4.4. Effect of solar intensity

Solar intensity is another significant parameter that affects system performance. Figs. 9 and 10 demonstrate the solar intensity's influence on the capital cost rate, exergy efficiency, output power, hydrogen, and oxygen production. Overall, the solar intensity improves the system efficiency and output power. An increase in solar intensity boosts the mass flow rate into the solar energy system and the gas turbine, thereby enhancing the SRC and ORC output power throughout the system along with increasing the system losses. The rise in overall power output leads to exergy efficiency enhancement by almost 10%. Similarly, the increase in the power output results in a spike in the capital costs from almost 170 to 305 $/h. Given that the PEM electrolyzer is powered by the SC and ORC output, an increase in their output power boosts hydrogen and oxygen production.

4.5. Effect of the number of heliostats

Figs. 11 and 12 show the effect of the number of heliostats on the system performance. Adding more heliostats can step up the energy rate

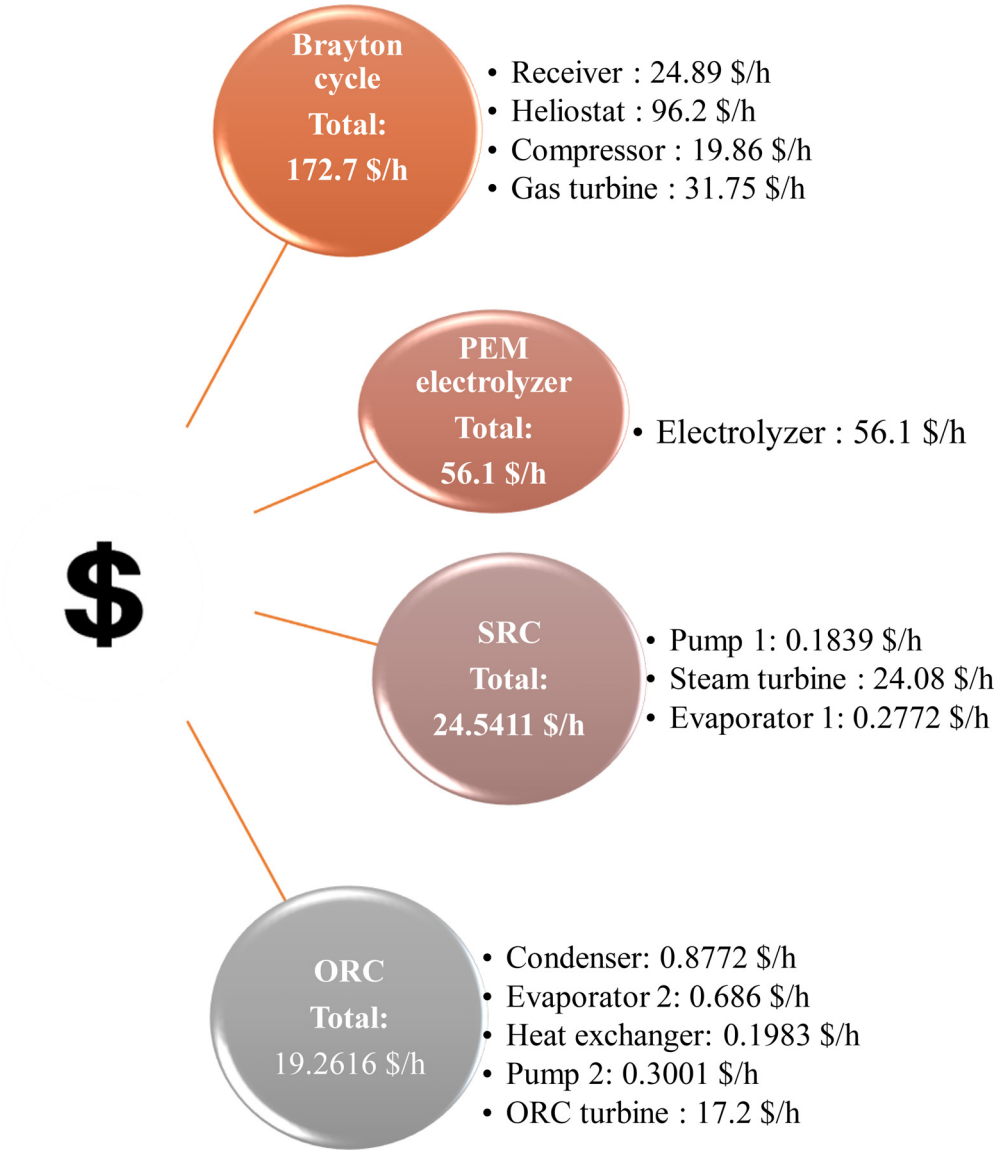

Fig. 18. Cost rate for each component.

through the system and improve the net power output. However, being an expensive component, heliostats exact a considerable toll on investors. Therefore, exergy efficiency improvement caused by increasing the number of heliostats comes at the expense of a substantial amount of money. Looking at Fig. 11, evidently, the rate of exergy efficiency improvement reduces when the number of heliostats gets high. The reason for this lies in the assumption of taking the temperature of output fluid from the solar tower (T_3) constant. In fact, by increasing the number of heliostats, the mass flow rate increases to keep T_3 constant, which results in more losses and a reduction in exergy efficiency improvement rate.

4.6. Effect of inlet and outlet pressure of SRC turbine

In this section, several contours are represented to assess the impact of SRC turbine inlet and outlet pressure on the system performance simultaneously. As shown in Fig. 13, having the pressure ratios around 30 with an inlet pressure of 3000 results in the highest system performance. It is worth mentioning that, according to Fig. 13 a and c, at the same pressure ratios, those with the least numerator (inlet pressure) and denominator (outlet pressure) perform at higher exergy efficiency and produce more power. However, this slightly higher exergy efficiency and power output are achieved at the expense of a higher cost ratio.

4.7. Effect of the ORC turbine inlet and outlet pressure on system performance

According to Fig. 14, contrary to the SRC turbine whose best exergy performance happened to be at the least amount of the inlet and output pressures for similar pressure ratios, the ORC turbine best performance takes place at the highest inlet and outlet pressures. On the other hand, although like SRC turbine, in the ORC turbine, the impact of inlet and outlet pressures on exergy efficiency is negligible, this improvement exacts higher costs to the investor.

4.8. Exergy destruction

The proportion of each component accounting for a specific amount of exergy destruction is shown in Fig. 15. Looking at the pie chart, it can be comprehended that the Brayton cycle is by far the most exergy-destructive element with destroying 88% of the total exergy destruction of the proposed system. The solar-related components, including receivers and heliostats, are responsible for most of the exergy destruc-

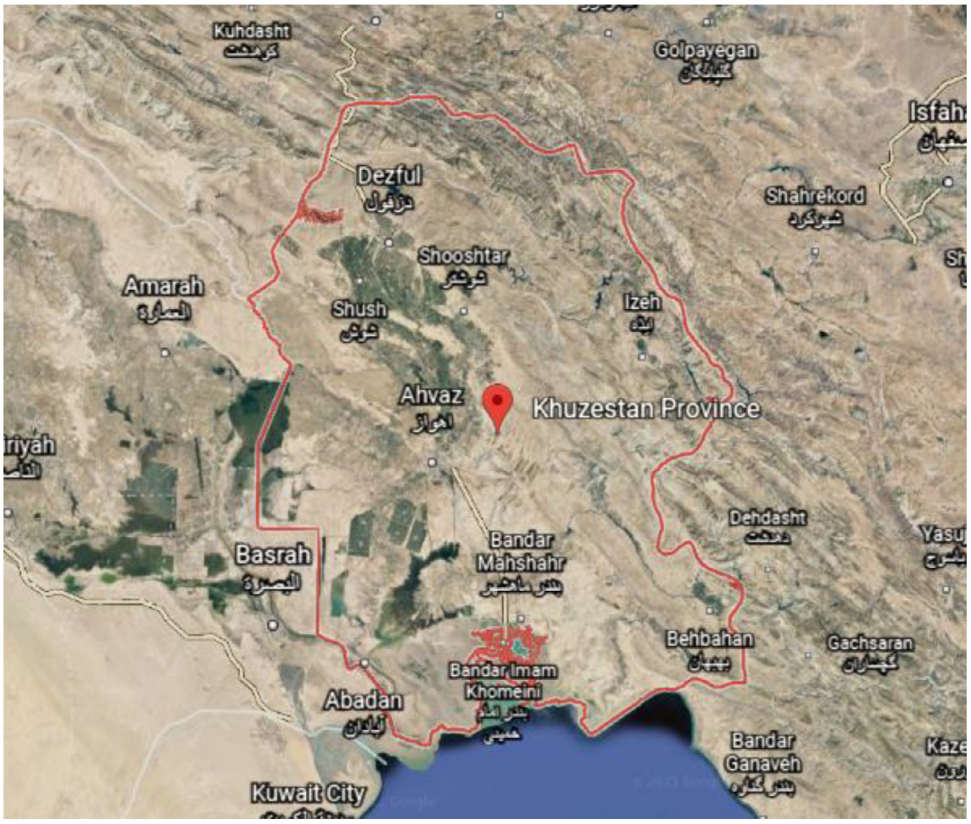

Fig. 19. Location of studied cities.

tion in the gas cycle. The PEM electrolyzer is ranked the second most exergy destructor, followed by the waste sections. For the sake of clarity, the specific amounts of exergy destruction in other components are also provided.

5. Optimization

Optimization has always been of crucial importance in improving efficiency and reducing costs. Recent progress made in numerical methods has led to several newly emerged optimization methods. While there are different types of optimizations, for instance, single-objective or multi-objective, they both follow almost the same procedure, distinguished in that multi-objective optimizations deal with more variables and objective functions. Several individual and often conflicting objectives ought to be fulfilled simultaneously to carry out a multi-objective optimization problem. These methods are used to find a set of optimum solutions or the Pareto frontier. Such an accurate method the NSGA-II that it is widely applied in multi-objective optimization algorithms. Aside from the numerous applications of NSGA-II, this method can be regarded as a standard that laid the groundwork for several other multi-objective optimization algorithms to be developed. This algorithm's unique approach to the multi-objective optimization process has been repeatedly exploited to develop new optimization algorithms. This algorithm is used in the present study to optimize a set of parameters and objective functions. The optimization enhances the efficiency of exergy and reduces the capital cost rate. A code is developed to couple the EES software with MATLAB through the Dynamic Data Exchange (DDE) protocol [5]. After a deep investigation of the effect of changes in various parameters on system performance, 6 design variables are selected to be optimized. Design variables considered in the optimization include the compressor pressure ratio (r_p), number of heliostat mirrors (N_{hel}) inlet pressure of turbine 2 (P_7), outlet pressure of SRC turbine (P_8), inlet temperature of ORC turbine (T_{11}), and evaporator pinch point temperature difference (PP_{Eva}). Table 4 presents the parameter range for each variable.

Table 5
The value of objective functions at optimum point.

22.2%	**Exergy efficiency**
272.6 $/h	**Total cost rate**

Table 6
The value of design parameters at optimum point.

Optimum value	Design parameter
9.67	$\mathbf{r_p}$
315	$\mathbf{N_{hel}}$
2783.9	$\mathbf{P_7}$
99.5	$\mathbf{P_8}$
86.2	$\mathbf{T_{11}}$
5.07	$\mathbf{PP_{Eva}}$

The illustrated Pareto frontier in Fig. 16 represents the optimal points for objective functions, exergy efficiency and cost rate. A rage of optimal solutions are provided by Fig. 16. While some points are better options from an economic point of view, they cannot be the final best possible option as exergy efficiency is at its lowest amount. Similarly, some points with high exergy efficiency cannot be a perfect answer since their high exergy efficiency have been achieved at a high value. Eventually, the ideal point is selected as the ultimate optimum point by TOPSIS decision making approach. The results from optimization are presented in Tables 5 and 6.

To provide a deeper intuition into optimum values, the scatter distribution of decision variables is represented in Fig. 17. While the optimum values for N_{hel}, P_7, P_8, PP_{EVA} are steadily distributed between the upper

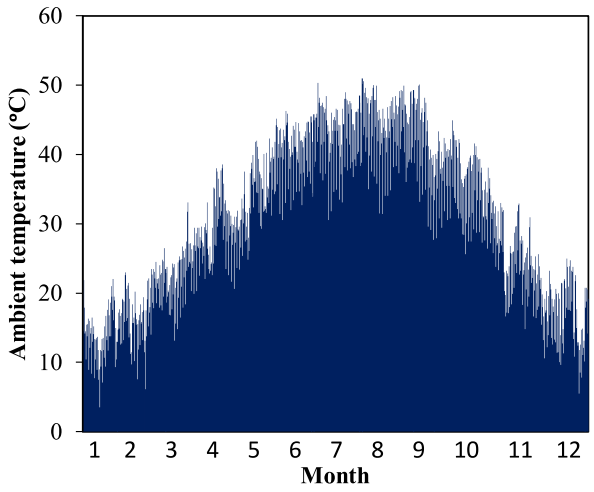

b) Ambient temperature variation in Abadan city

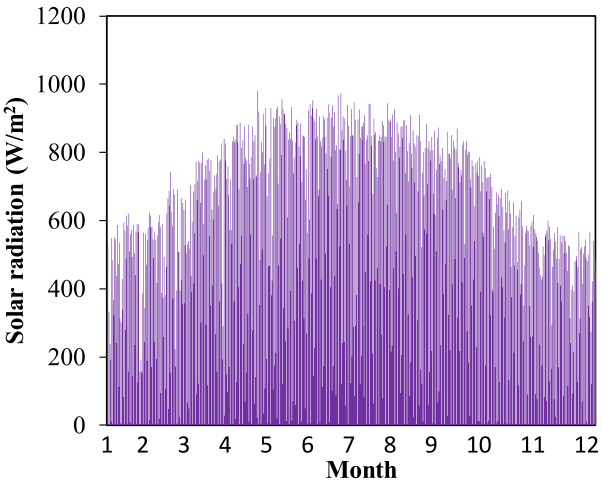

a) Solar radiation variation in Abadan city

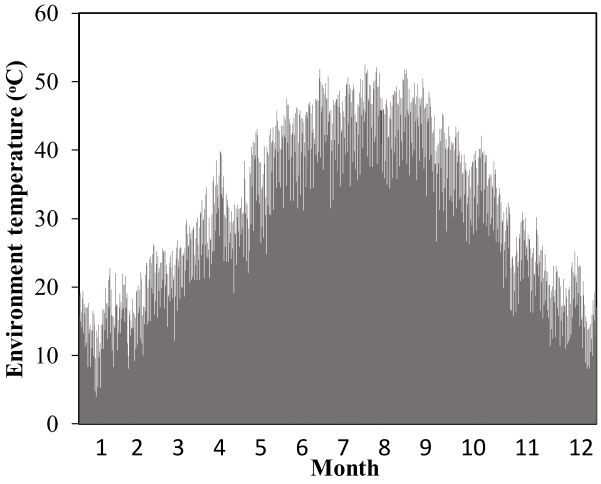

d) Ambient temperature variation in Dezful city

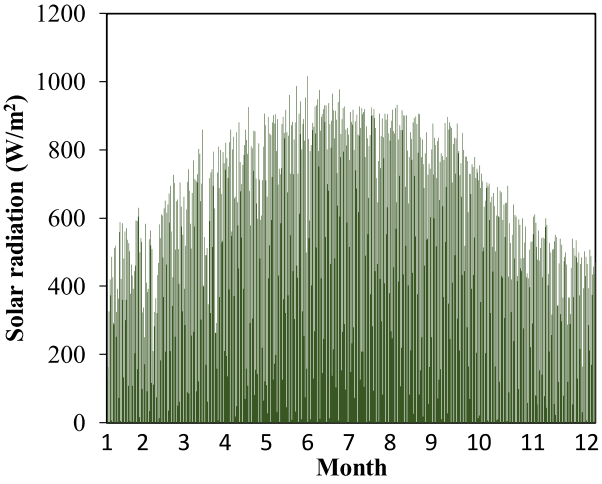

c) Solar radiation variation in Dezful city

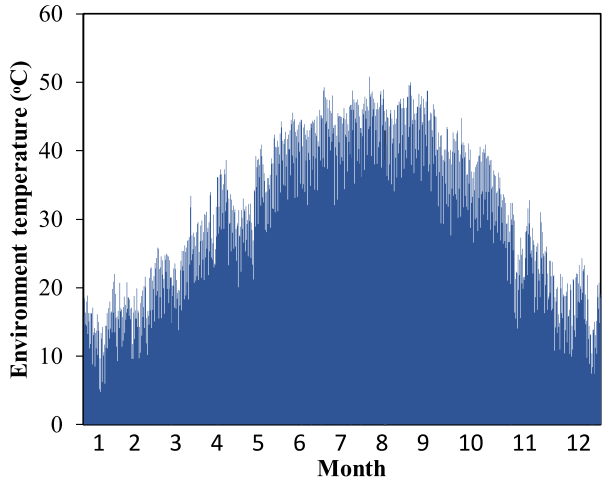

f) Ambient temperature variation in Ahvaz city

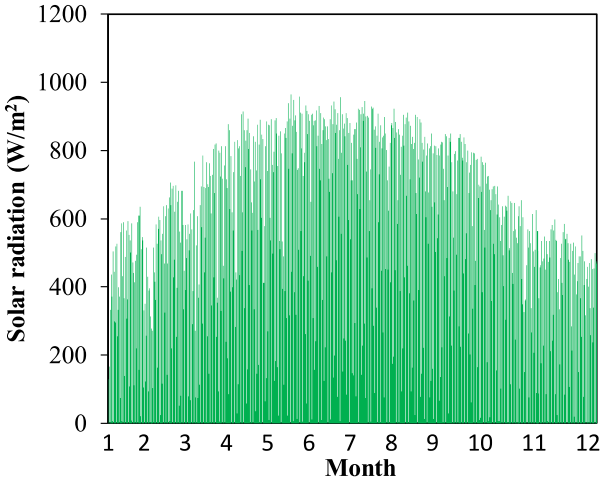

e) Solar radiation variation in Ahvaz city

Fig. 20. Variations of ambient temperature and solar radiation during a year.

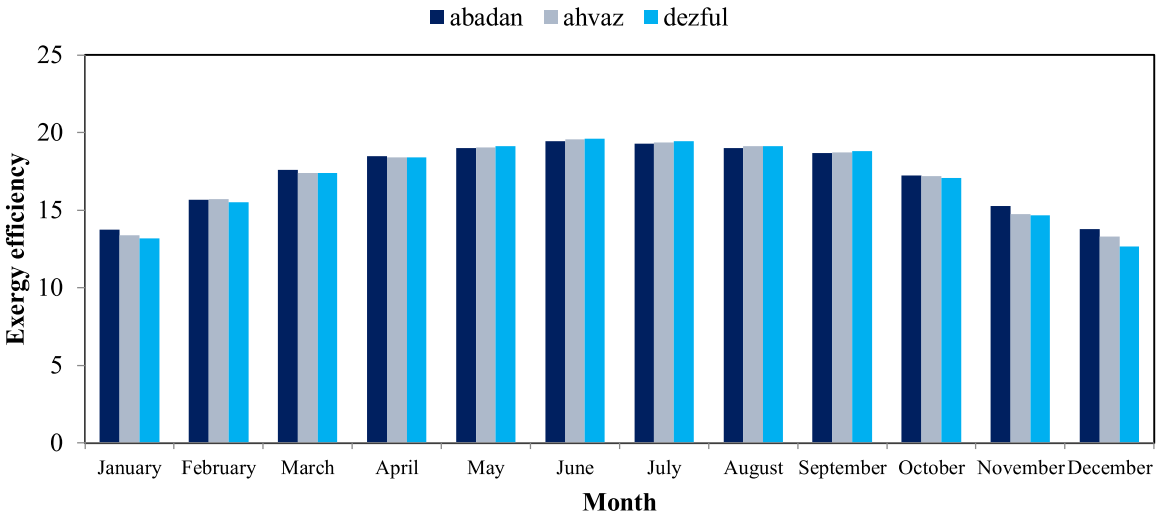

Fig. 21. Effect of variations of solar intensity during a year on exergy efficiency for studied areas.

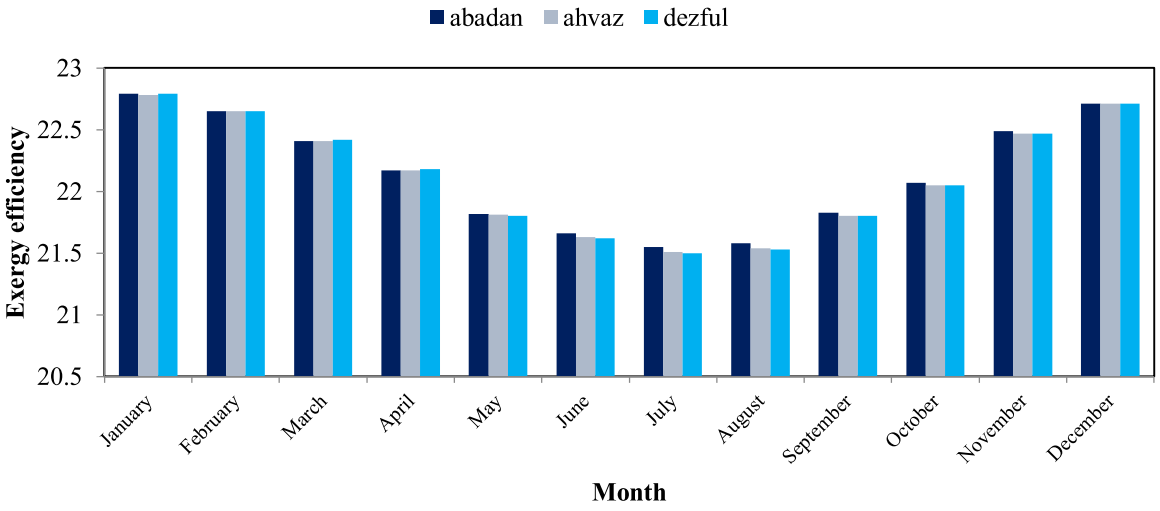

Fig. 22. Effect of variations of ambient temperature during a year on exergy efficiency for studied areas.

and lower bounds, the optimum values for r_p and T_{11} are mostly around one specific amount.

Lastly, a cost analysis is presented in Fig. 18 to show the share of each component on the total system costs (272.6027 $/h) at optimum conditions. According to the figure, the Brayton cycle and PEM electrolyzer account for up to 83% of system costs.

6. Case study (Khuzestan province, Iran)

The effect of solar radiation and ambient temperature in these cities on the system performance is evaluated in this section. Khuzestan province in the southwest of Iran holds a striking solar potential due to the abundance of solar radiation all year round. For this reason, three major cities located in this area – namely Abadan, Ahvaz, and Dezful - are considered to explore the best option for implementation of the studied system. Fig. 19 shows the location of these mentioned cities. The meteorological data for these cities is used to evaluate the system performance at its optimal design condition.

Fig. 20 illustrates the variation of solar radiation and ambient temperature throughout the year in 3 studied cities.

Figs. 21 and 22 demonstrate how solar irradiation and ambient temperature affect the exergy efficiency. According to Fig. 21, the highest exergy efficiency takes place in June and July – the hottest months of the year, when the sun shines intensely- because based on Fig. 9 the higher solar irradiation is, the more exergy efficiency would be. Contrary to the solar intensity which positively affects exergy efficiency, based on Fig. 22, ambient temperature diminishes exergy efficiency. Therefore, its least value occurs during June and July.

The reason for the system's weaker performance at high ambient temperatures is the compressor. Fig. 23 proves that the exergy efficiency goes down for constant pressure ratios when the temperature increases. In fact, at high ambient temperatures the specific volume of the working fluid increases; consequently, more power is consumed by the compressor to maintain the same discharge pressure. This increase in consumption of gas turbine work significantly reduces the net generated work and exergy efficiency.

According to Fig. 24, due to the positive correlation between power production and solar irradiation, the system generated power and work peak is during June and July. As mentioned before, at high ambient temperatures, the compressor consumes more work so that the system's net power output behavior is so similar to the exergy efficiency, and this issue is demonstrated in Fig. 25.

The impact of the solar irradiation and ambient temperature on hydrogen production are shown in Figs. 26 and 27. Contrary to exergy efficiency and power generation, hydrogen production shows similar behavior under the influence of solar irradiation and ambient temperature. While the power generation is at its lowest amount during June

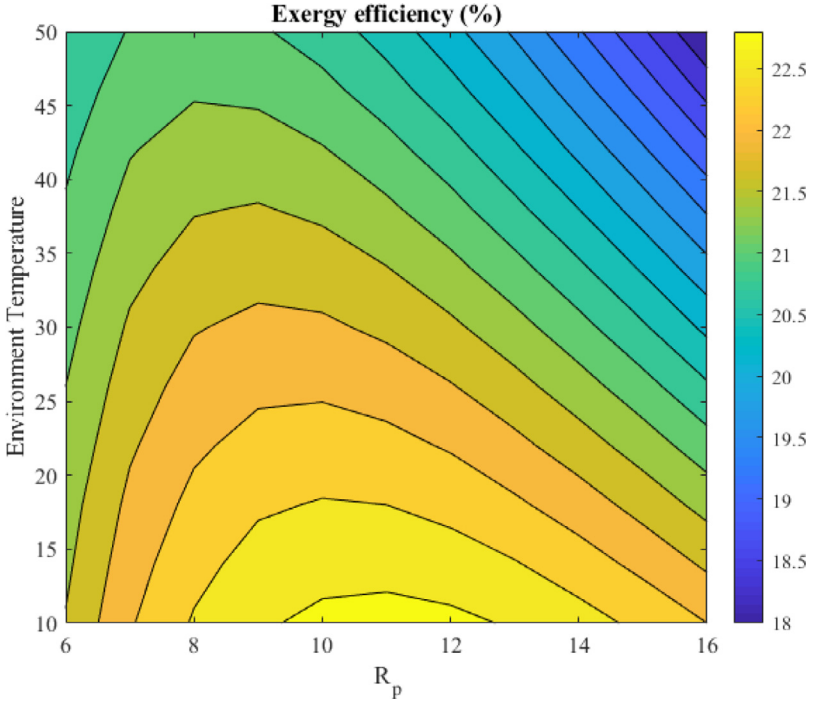

Fig. 23. Effect of compressor pressure ratio and ambient temperature on the exergy efficiency.

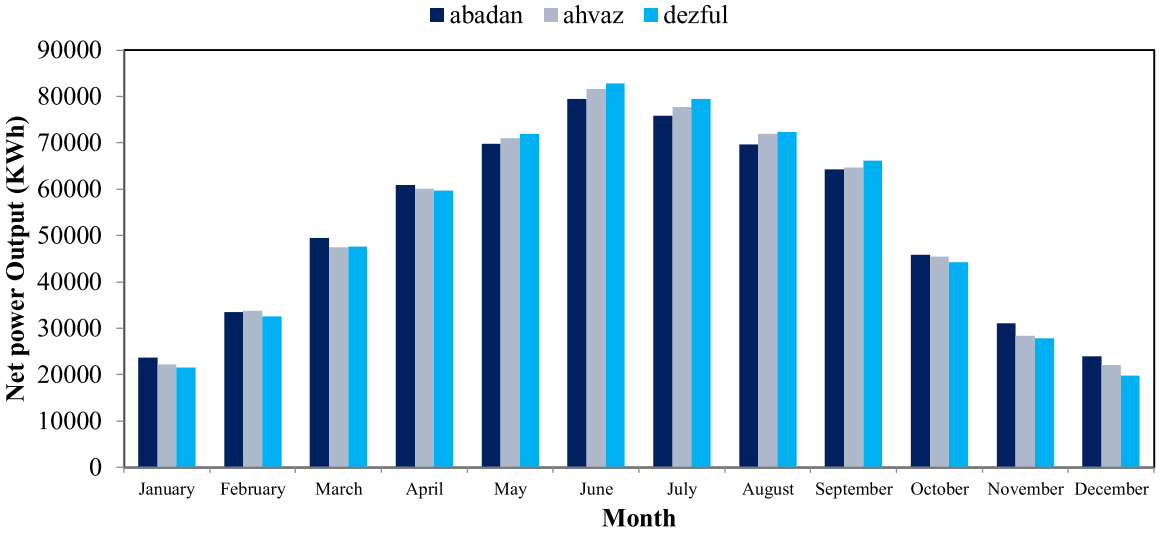

Fig. 24. Effect of variations of solar intensity during a year on net work output for studied areas.

and July, the PEM electrolyzer performance is enhanced during these two months. The reason for this rather unexpected behavior is the performance of SRC and ORC, which are responsible for providing PEM electrolyzer with energy. Their better performance during June and July results in higher hydrogen (and oxygen) production during the summer time. However, the Brayton cycle still delivers a lower amount of electricity during these two months.

Overall, implementation of such green concept hybrid energy systems has opened up a window involving water-sunlight-energy to properly use waste energies for efficiency improvement and pollution reduction. However, to stimulate the installation of integrated systems, they should be comprehensively explored. This study aimed to investigate technical aspects of a novel cogeneration system to enable higher penetration of clean-based energy systems.

7. Conclusion

In this study, a unique integrated energy-generating system hinged on CSP was introduced with the upshot of producing power, hydrogen, and oxygen. EES, an engineering software, is utilized in an attempt to conduct the modeling and thermo-economic analysis of the proposed system. Concerning the significant share of a solar field in destroying the exergy, the urge to address this issue in the future is evident. After evaluating the impact of various parameters, the results were optimized in an unprecedented approach using the multi-objective NSGA-II. The use of the TOPSIS approach selected the best-operating condition on a Pareto frontier. Lastly, the impact of ambient temperature and solar irradiation on the system performance were investigated. In short, the notable results are summed up as below:

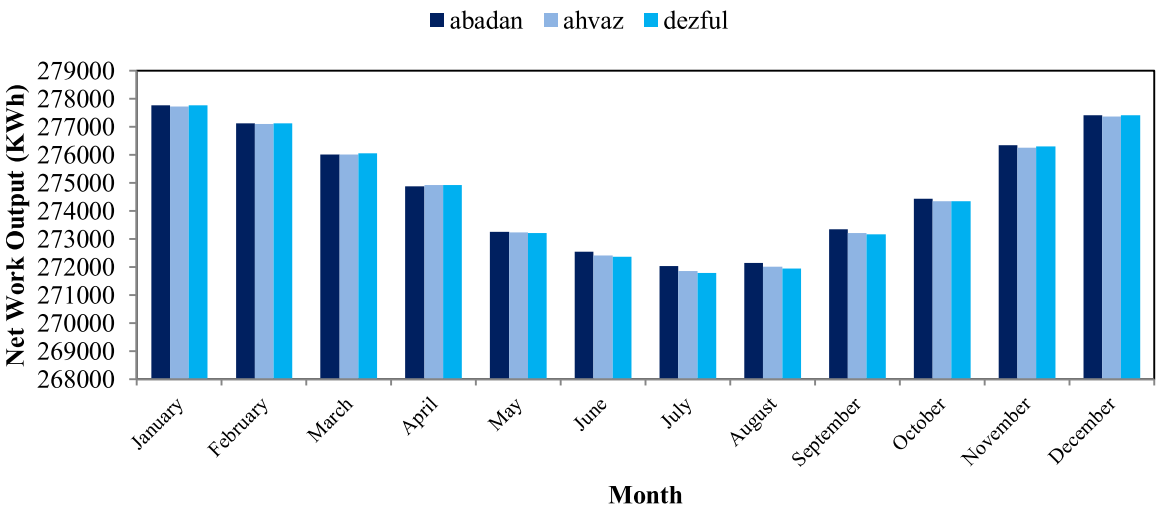

Fig. 25. Effect of changes in ambient temperature during a year on net work output for studied areas.

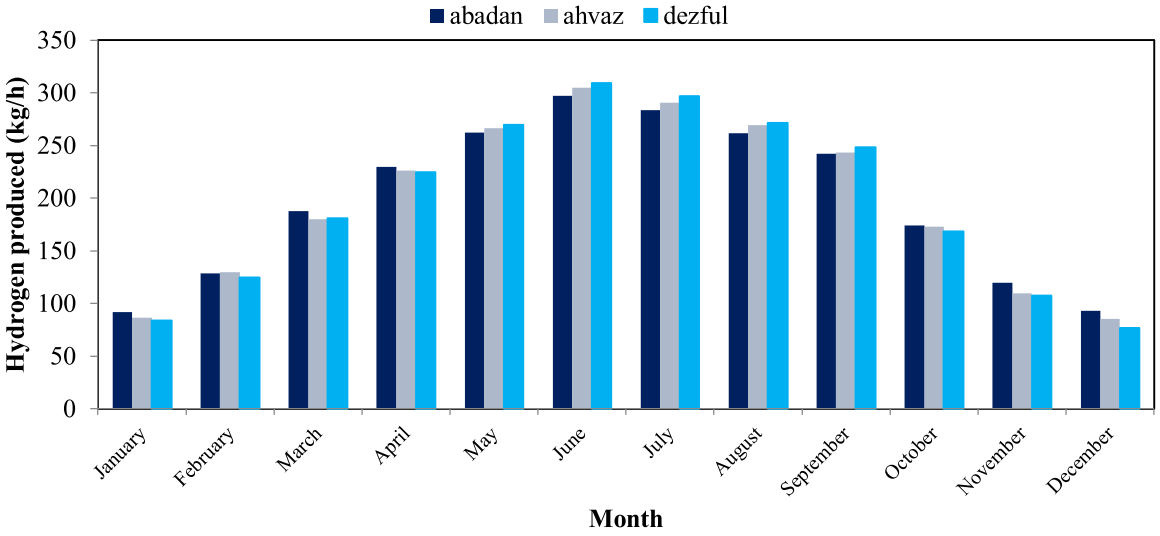

Fig. 26. Effect of variations of solar intensity during a year on hydrogen production for studied areas.

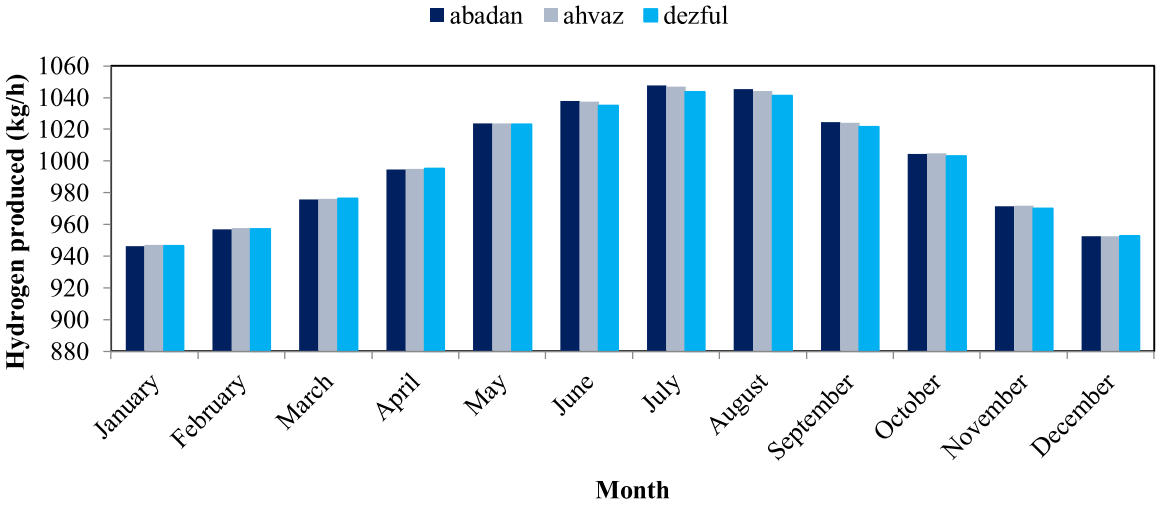

Fig. 27. Effect of changes in ambient temperature during a year on net power output for studied areas.

- A higher solar intensity can significantly increase the overall output power as well as the costs.
- Based on the results, the solar field accounted for the highest exergy destruction.
- At the optimum point picked by TOPSIS method, the system offers an exergy efficiency of 22.2% and a capital cost rate of 272.6 $/h.
- Brayton cycle and solar field is responsible for the majority of the system's costs.
- Between the ambient temperature and solar irradiation, the latter has the dominant effect.

Declaration of Competing Interest

The authors declare that they have no known competing financial interests or personal relationships that could have appeared to influence the work reported in this paper.

Acknowledgement

We are grateful to Prof. Huan Xi from Xi'an Jiaotong University who gave up several hours of his valuable time to provide us with his constructive comments.

References

[1] F Yilmaz, Thermodynamic performance evaluation of a novel solar energy based multigeneration system, Appl. Therm. Eng. 143 (2018) 429–437, doi:10.1016/j.applthermaleng.2018.07.125.
[2] S. Bashiri Mousavi, M. Adib, M. Soltani, A.R. Razmi, J Nathwani, Transient thermodynamic modeling and economic analysis of an adiabatic compressed air energy storage (A-CAES) based on cascade packed bed thermal energy storage with encapsulated phase change materials, Energy Convers. Manag. 243 (2021) 114379, doi:10.1016/j.enconman.2021.114379.
[3] A. Behzadi, A Arabkoohsar, Comparative performance assessment of a novel cogeneration solar-driven building energy system integrating with various district heating designs, Energy Convers. Manag. 220 (2020) 113101, doi:10.1016/j.enconman.2020.113101.
[4] J. Dai, S. Wu, G. Han, J. Weinberg, X. Xie, X. Wu, et al., Water-energy nexus: a review of methods and tools for macro-assessment, Appl. Energy 210 (2018) 393–408, doi:10.1016/J.APENERGY.2017.08.243.
[5] S.M. Alirahmi, S. Rahmani Dabbagh, P. Ahmadi, S Wongwises, Multi-objective design optimization of a multi-generation energy system based on geothermal and solar energy, Energy Convers. Manag. 205 (2020) 112426, doi:10.1016/j.enconman.2019.112426.
[6] M.T. Islam, N. Huda, A.B. Abdullah, R Saidur, A comprehensive review of state-of-the-art concentrating solar power (CSP) technologies: current status and research trends, Renew Sustain Energy Rev 91 (2018) 987–1018, doi:10.1016/j.rser.2018.04.097.
[7] A. Behzadi, E. Gholamian, P. Ahmadi, A. Habibollahzade, M Ashjaee, Energy, exergy and exergoeconomic (3E) analyses and multi-objective optimization of a solar and geothermal based integrated energy system, Appl. Therm. Eng. 143 (2018) 1011–1022, doi:10.1016/j.applthermaleng.2018.08.034.
[8] A. Behzadi, A. Arabkoohsar, E Gholamian, Multi-criteria optimization of a biomass-fired proton exchange membrane fuel cell integrated with organic rankine cycle/thermoelectric generator using different gasification agents, Energy 201 (2020) 117640, doi:10.1016/j.energy.2020.117640.
[9] E. Assareh, M. Assareh, S.M. Alirahmi, S. Jalilinasrabady, A. Dejdar, M Izadi, An extensive thermo-economic evaluation and optimization of an integrated system empowered by solar-wind-ocean energy converter for electricity generation – case study: Bandar ABAS, Iran, Therm. Sci. Eng. Prog. 25 (2021) 100965, doi:10.1016/j.tsep.2021.100965.
[10] S. Muhammad-Bashir, M. Al-Oufi, M. Al-Hakami, M.A. Nadeem, K. Mudiyanselage, H Idriss, Comparison between the performance of high concentrated and non-concentrated PV-cells for hydrogen production using PEM water electrolyzers, Sol. Energy 205 (2020) 461–464, doi:10.1016/j.solener.2020.05.077.
[11] M.M. Aboelmaaref, M.E. Zayed, J. Zhao, W. Li, A.A. Askalany, M. Salem Ahmed, et al., Hybrid solar desalination systems driven by parabolic trough and parabolic dish CSP technologies: technology categorization, thermodynamic performance and economical assessment, Energy Convers. Manag. 220 (2020) 113103, doi:10.1016/j.enconman.2020.113103.
[12] T.E. Boukelia, A. Bouraoui, A. Laouafi, S. Djimli, Y Kabar, 3E (energy-exergy-economic) comparative study of integrating wet and dry cooling systems in solar tower power plants, Energy 200 (2020) 117567, doi:10.1016/j.energy.2020.117567.
[13] S. Anvari, S. Khalilarya, V Zare, Power generation enhancement in a biomass-based combined cycle using solar energy: thermodynamic and environmental analysis, Appl. Therm. Eng. 153 (2019) 128–141, doi:10.1016/j.applthermaleng.2019.02.112.
[14] S. Riahi, M. Liu, R. Jacob, M. Belusko, F Bruno, Assessment of exergy delivery of thermal energy storage systems for CSP plants: cascade PCMs, graphite-PCMs and two-tank sensible heat storage systems, Sustain. Energy Technol. Assess. 42 (2020) 100823, doi:10.1016/j.seta.2020.100823.
[15] C. Prieto, L.F Cabeza, Thermal energy storage (TES) with phase change materials (PCM) in solar power plants (CSP). Concept and plant performance, Appl. Energy 254 (2019) 113646, doi:10.1016/j.apenergy.2019.113646.
[16] K.E. Elfeky, X. Li, N. Ahmed, L. Lu, Q Wang, Optimization of thermal performance in thermocline tank thermal energy storage system with the multilayered PCM(s) for CSP tower plants, Appl. Energy 243 (2019) 175–190, doi:10.1016/j.apenergy.2019.03.182.
[17] B. Ghorbani, R. Shirmohammadi, M Mehrpooya, Development of an innovative cogeneration system for fresh water and power production by renewable energy using thermal energy storage system, Sustain. Energy Technol. Assess. 37 (2020) 100572, doi:10.1016/j.seta.2019.100572.
[18] M. Ozturk, I. Dincer, N Javani, Thermodynamic modeling of a solar energy based combined cycle with rock bed heat storage system, Sol. Energy 200 (2020) 51–60, doi:10.1016/j.solener.2019.03.053.
[19] A. Vinca, K. Riahi, A. Rowe, N Djilali, Climate-land-energy-water nexus models across scales: progress, gaps and best accessibility practices, Front. Environ. Sci. 0 (2021) 252, doi:10.3389/FENVS.2021.691523.
[20] H Mehrjerdi, Modeling and optimization of an island water-energy nexus powered by a hybrid solar-wind renewable system, Energy 197 (2020) 117217, doi:10.1016/J.ENERGY.2020.117217.
[21] A. Baldinelli, L. Barelli, G. Bidini, G. Cinti, A. Di Michele, F Mondi, How to power the energy–water nexus: coupling desalination and hydrogen energy storage in mini-grids with reversible solid oxide cells, Processes 8 (2020) 1–22, doi:10.3390/pr8111494.
[22] S.M. Alirahmi, E. Assareh, A. Chitsaz, S. Ghazanfari Holagh, S Jalilinasrabady, Electrolyzer-fuel cell combination for grid peak load management in a geothermal power plant: power to hydrogen and hydrogen to power conversion, Int. J. Hydrog. Energy 46 (2021) 25650–25665, doi:10.1016/j.ijhydene.2021.05.082.
[23] F. Razi, I. Dincer, K Gabriel, Exergoenvironmental analysis of the integrated copper-chlorine cycle for hydrogen production, Energy 226 (2021) 120426, doi:10.1016/j.energy.2021.120426.
[24] S. Sadeghi, S. Ghandehariun, G.F Naterer, Exergoeconomic and multi-objective optimization of a solar thermochemical hydrogen production plant with heat recovery, Energy Convers. Manag. 225 (2020) 113441, doi:10.1016/j.enconman.2020.113441.
[25] S.M. Alirahmi, E. Assareh, N.N. Pourghassab, M. Delpisheh, L. Barelli, A Baldinelli, Green hydrogen & electricity production via geothermal-driven multi-generation system: thermodynamic modeling and optimization, Fuel 308 (2022) 122049, doi:10.1016/j.fuel.2021.122049.
[26] S. Sharma, S. Basu, N.P. Shetti, T.M Aminabhavi, Waste-to-energy nexus for circular economy and environmental protection: recent trends in hydrogen energy, Sci. Total Environ. 713 (2020) 136633, doi:10.1016/J.SCITOTENV.2020.136633.
[27] S.M. Alirahmi, A.R. Razmi, A Arabkoohsar, Comprehensive assessment and multi-objective optimization of a green concept based on a combination of hydrogen and compressed air energy storage (CAES) systems, Renew. Sustain. Energy Rev. 142 (2021) 110850, doi:10.1016/j.rser.2021.110850.
[28] S. Marami Milani, R. Khoshbakhti Saray, M Najafi, Exergo-economic analysis of different power-cycle configurations driven by heat recovery of a gas engine, Energy Convers. Manag. 186 (2019) 103–119, doi:10.1016/j.enconman.2019.02.030.
[29] M.H. Nabat, M. Zeynalian, A.R. Razmi, A. Arabkoohsar, M Soltani, Energy, exergy, and economic analyses of an innovative energy storage system; liquid air energy storage (LAES) combined with high-temperature thermal energy storage (HTES), Energy Convers. Manag. 226 (2020) 113486, doi:10.1016/j.enconman.2020.113486.
[30] M. Soltani, M.H. Nabat, A.R. Razmi, M.B. Dusseault, J Nathwani, A comparative study between ORC and Kalina based waste heat recovery cycles applied to a green compressed air energy storage (CAES) system, Energy Convers. Manag. 222 (2020) 113203, doi:10.1016/j.enconman.2020.113203.
[31] I. Fakhari, A. Behzadi, E. Gholamian, P. Ahmadi, A Arabkoohsar, Comparative double and integer optimization of low-grade heat recovery from PEM fuel cells employing an organic Rankine cycle with zeotropic mixtures, Energy Convers. Manag. 228 (2021) 113695, doi:10.1016/j.enconman.2020.113695.
[32] F. Moradi Nafchi, E. Baniasadi, E. Afshari, N Javani, Performance assessment of a solar hydrogen and electricity production plant using high temperature PEM electrolyzer and energy storage, Int. J. Hydrog. Energy 43 (2018) 5820–5831, doi:10.1016/j.ijhydene.2017.09.058.
[33] A. Salehi, S.M. Mousavi, A. Fasihfar, M Ravanbakhsh, Energy, exergy, and environmental (3E) assessments of an integrated molten carbonate fuel cell ({MCFC}), Stirling engine and organic Rankine cycle ({ORC}) cogeneration system fed by a biomass-fueled gasifier, Int. J. Hydrogen Energy 44 (2019) 31488–31505, doi:10.1016/j.ijhydene.2019.10.038.
[34] J. Rouleau, L Gosselin, Impacts of the COVID-19 lockdown on energy consumption in a Canadian social housing building, Appl. Energy 287 (2021) 116565, doi:10.1016/j.apenergy.2021.116565.
[35] S.M. Alirahmi, M. Rostami, A.H Farajollahi, Multi-criteria design optimization and thermodynamic analysis of a novel multi-generation energy system for hydrogen, cooling, heating, power, and freshwater, Int. J. Hydrog. Energy 45 (2020) 15047–15062, doi:10.1016/j.ijhydene.2020.03.235.
[36] P. Ahmadi, I. Dincer, M.A Rosen, Energy and exergy analyses of hydrogen production via solar-boosted ocean thermal energy conversion and PEM electrolysis, Int. J. Hydrog. Energy 38 (2013) 1795–1805, doi:10.1016/j.ijhydene.2012.11.025.

[37] A.S. Nafey, M.A Sharaf, Combined solar organic Rankine cycle with reverse osmosis desalination process: energy, exergy, and cost evaluations, Renew. Energy 35 (2010) 2571–2580, doi:10.1016/j.renene.2010.03.034.
[38] Kotas T. The exergy method of thermal plant analysis. 2013.
[39] S.M. Alirahmi, S. Bashiri Mousavi, A.R. Razmi, P Ahmadi, A comprehensive techno-economic analysis and multi-criteria optimization of a compressed air energy storage (CAES) hybridized with solar and desalination units, Energy Convers. Manag. 236 (2021) 114053, doi:10.1016/j.enconman.2021.114053.
[40] M.E. Demir, I Dincer, Development of a hybrid solar thermal system with TEG and PEM electrolyzer for hydrogen and power production, Int. J. Hydrog. Energy 42 (2017) 30044–30056, doi:10.1016/j.ijhydene.2017.09.001.
[41] I. Dincer, C Acar, Review and evaluation of hydrogen production methods for better sustainability, Int. J. Hydrog. Energy 40 (2014) 11094–11111, doi:10.1016/j.ijhydene.2014.12.035.
[42] Y. Cengel, M Boles, Thermodynamics: An Engineering Approach, 6th ed., SI Units, 2007.
[43] M. Ni, M.K.H. Leung, D.Y.C Leung, Energy and exergy analysis of hydrogen production by a proton exchange membrane (PEM) electrolyzer plant, Energy Convers. Manag. 49 (2008) 2748–2756, doi:10.1016/j.enconman.2008.03.018.
[44] A. Behzadi, A. Habibollahzade, P. Ahmadi, E. Gholamian, E Houshfar, Multi-objective design optimization of a solar based system for electricity, cooling, and hydrogen production, Energy 169 (2019) 696–709, doi:10.1016/j.energy.2018.12.047.
[45] A. Ebrahimi-Moghadam, A.J. Moghadam, M. Farzaneh-Gord, K Aliakbari, Proposal and assessment of a novel combined heat and power system: energy, exergy, environmental and economic analysis, Energy Convers. Manag. 204 (2020) 112307, doi:10.1016/j.enconman.2019.112307.
[46] A. Ebrahimi-Moghadam, A.J. Moghadam, M Farzaneh-Gord, Comprehensive techno-economic and environmental sensitivity analysis and multi-objective optimization of a novel heat and power system for natural gas city gate stations, J. Clean. Prod. 262 (2020) 121261, doi:10.1016/j.jclepro.2020.121261.
[47] S.M. Alirahmi, S.F. Mousavi, P. Ahmadi, A Arabkoohsar, Soft computing analysis of a compressed air energy storage and SOFC system via different artificial neural network architecture and tri-objective grey wolf optimization, Energy 236 (2021) 121412, doi:10.1016/j.energy.2021.121412.
[48] A. Ebrahimi-Moghadam, A. Jabari Moghadam, M. Farzaneh-Gord, A Arabkoohsar, Performance investigation of a novel hybrid system for simultaneous production of cooling, heating, and electricity, Sustain. Energy Technol. Assess. 43 (2021) 100931, doi:10.1016/j.seta.2020.100931.
[49] Z. Li, S. Khanmohammadi, S. Khanmohammadi, A.A.A.A. Al-Rashed, P. Ahmadi, M Afrand, 3-E analysis and optimization of an organic rankine flash cycle integrated with a PEM fuel cell and geothermal energy, Int. J. Hydrog. Energy (2019), doi:10.1016/j.ijhydene.2019.09.233.
[50] A.R. Razmi, M Janbaz, Exergoeconomic assessment with reliability consideration of a green cogeneration system based on compressed air energy storage (CAES), Energy Convers. Manag. 204 (2020) 112320, doi:10.1016/j.enconman.2019.112320.
[51] P. Ahmadi, I. Dincer, M.A Rosen, Multi-objective optimization of a novel solar-based multigeneration energy system, Sol. Energy 108 (2014) 576–591, doi:10.1016/j.solener.2014.07.022.
[52] E. Akrami, A. Chitsaz, H. Nami, S.M.S Mahmoudi, Energetic and exergoeconomic assessment of a multi-generation energy system based on indirect use of geothermal energy, Energy 124 (2017) 625–639, doi:10.1016/j.energy.2017.02.006.
[53] T. Ioroi, K. Yasuda, Z. Siroma, N. Fujiwara, Y Miyazaki, Thin film electrocatalyst layer for unitized regenerative polymer electrolyte fuel cells, J. Power Sources 112 (2002) 583–587, doi:10.1016/S0378-7753(02)00466-4.